Sedimentary Geology 460 (2024) 106563

Contents lists available at ScienceDirect

Sedimentary Geology

journal homepage: www.elsevier.com/locate/sedgeo

Testing the record of climate-related cyclicity in microbial lamination: An example from Miocene oncolites in the Ebro Basin, Spain

F.J. Pérez-Rivarés [a,c], G. Pardo [a], C. Arenas [a,b,c,*]

[a] Department of Earth Sciences, University of Zaragoza, 50009 Zaragoza, Spain
[b] Institute for Research on Environmental Sciences of Aragón (IUCA), Spain
[c] Geotransfer Group, University of Zaragoza, 50009 Zaragoza, Spain

ARTICLE INFO

Article history:
Received 16 November 2023
Received in revised form 14 December 2023
Accepted 16 December 2023
Available online 22 December 2023

Editor: Dr. Catherine Chagué

Keywords:
Microbial lamination
Spectral analysis
Periodicity
Lacustrine and fluvial oncolites
Solar cycles

ABSTRACT

This work tests the relationship between quasi-periodic climate-linked parameters and cyclicity recorded through microbial lamination using spectral analysis of time series based on lamina thickness and luminance, as well as C and O stable isotope data. Three oncolites of the Ebro Basin were used: specimens C4-1 and C4-31 from a lacustrine bed dated at 13.8 My, and specimen VD-13 from a fluvial bed whose age is younger than 12 My. Lamination consists of alternating light and dark calcite laminae, which correspond to crystal size and porosity variations. Composite light and dark laminae can be seen by the naked eye. Spectral analysis based on the thickness and luminance measurements of simple light–dark lamina couplet successions revealed that the three specimens had recurrent periods of 2.5, 3 and 10–13. On the hypothesis that each simple light–dark lamina couplet represents a 1-year duration, the 2.5 and 10–13 periods can be related to the 2.5-year quasi-biennial oscillation and the 11-year Schwabe sunspot cycle, respectively. Other less frequent periods present around 5 and 7, together with period 3, could be related to the most typical modes of the North Atlantic Oscillation and/or El Niño Southern Oscillation. The periods at 19–23, present in specimen C4-31, can be correlated with the 22-year Hale sunspot cycle. The 10–13 and 19–23 periods were also detected using the $\delta^{13}C$ and $\delta^{18}O$ values of successive laminae in specimen C4-31. These data suggest that solar irradiance variations influenced the characteristics of the oncolite laminae, through temperature and precipitation. Although the studied oncolites do not present an optimal thickness lamination pattern for spectral analysis, their lamination is capable of registering periodic climatic variations, and these results provide further evidence that microbial laminations can serve as high-resolution records of climate and climate-linked cycles over different time scales.

1. Introduction

The climatic and environmental significance of textural variations in microbial laminae is a topic that has been debated for a long time (Monty, 1976; Casanova, 1994; Brasier et al., 2010; Suarez-Gonzalez et al., 2014; Arenas and Jones, 2017; Martin-Bello et al., 2019a). Reasons for the ongoing debate include the complexity derived from the different orders of cyclicity in most laminated microbialites, and the fact that the duration of the laminae is unknown for most ancient examples. Moreover, several factors influence the form and continuity of laminae. Microbial lamination results from the complex interaction of physical, chemical and biological parameters (Monty, 1976; Golubic, 1991; Merz-Preiß and Riding, 1999; Riding, 2000; Noffke and Awramik, 2013), which substantially depend on climate and hydrology (Arenas et al., 2015). First, the characteristics of the sedimentary environment, including hydrology and hydrodynamic features (i.e., depth, light and agitation), hydrochemistry (i.e., salinity, mineral saturation levels, and chemical compounds that affect biota) and the morphology of the substrate over which microbial mats develop. Second, the composition of biotic associations that refers to the attributes, physiological properties and morphological characteristics of the microbial species, primarily cyanobacteria. All these aspects can intervene on different spatial and temporal scales, producing a complex pattern of features that is difficult to disentangle.

A relationship between the solar activity cycles and the development of ancient laminated deposits has been widely claimed. The cyclicity shown by variations in lamination colour and thickness reported in some ancient laminated lacustrine records has been attributed to periodic variations in climatic conditions modulated by solar irradiance changes (Bradley, 1929; Ripepe et al., 1991; Muñoz et al., 2002b;

* Corresponding author at: Department of Earth Sciences, University of Zaragoza, 50009 Zaragoza, Spain.
E-mail address: carenas@unizar.es (C. Arenas).

https://doi.org/10.1016/j.sedgeo.2023.106563

Shunk et al., 2009; Lenz et al., 2010; Li et al., 2018; Pérez-Rivarés et al., 2019; Shi et al., 2021). Earlier studies interpreted cyclic changes in varve thickness from the oil shales of the Green River Formation, Eocene, USA, as records of sunspot cycles (Bradley, 1929, 1931; Crowley et al., 1986). Subsequently, climatic phenomena such as the El Niño Southern Oscillation (ENSO) were also suggested to be the origin of these systematic fluctuations (Ripepe et al., 1991). The evidence of solar cycles has also been recognised in Neogene lacustrine deposits through the spectral analysis of the varve thickness. For example, the 11-year Schwabe cycle has been identified in many cases (Muñoz et al., 2002b), together with the 22-year Hale cycle (Shunk et al., 2009), and in some cases, along with the 85 ± 15-year Gleissberg cycle (Shi et al., 2021). Similar solar cyclic patterns were observed in other ancient laminated facies, for example, for carbonate and siliciclastic bio-laminites related to past solar activity reported for the Precambrian (Tang et al., 2014; Li et al., 2018). In these studies, cyclicity based on lamina thickness and X-ray fluorescence or geochemical data was related to the 11-year Schwabe sunspot and 22-year solar Hale cycles.

In the aforementioned studies, alternating light and dark lamina couplets were identified as having annual origins. In most studies on ancient laminated microbialites the age assignment to the simple lamina cycles is typically tentative, either as a requirement for or owing to diverse interpretations, but their results do not evaluate the lamina duration. In Cretaceous lacustrine oncolites from New Zealand, Lindqvist (1994) noticed several orders of cyclicity in the laminae based on texture and thickness. This author suggested that couplets 50–500 μm thick were linked to seasonal variations in temperature and light intensity, and thicker groups of such couplets (~1.5 mm thick) could represent longer climate-induced lake-level and nutrient supply variations. Based on the textural and C and O isotope values of oncolites that developed in a Jurassic fluvial rift basin in northern Spain, Arenas et al. (2015) tentatively proposed a seasonal-to-pluriannual duration for dark and light composite laminae. Petrographic and C and O isotope results of Holocene lacustrine stromatolites in the East African Rift Valley led Casanova (1986, 1994) to propose that each light spar and dark micrite lamina couplet represents the response of the microbial mat to seasonal contrasts. The light laminae were linked to the rainy season, and the dark laminae to the dry season.

Unlike the aforementioned examples, studies based on the periodic monitoring of many recent tufa-depositing fluvial environments have demonstrated that the formation of porous and/or light spar laminae and dense and/or dark micrite laminae, both comprising cyanobacterial calcite tubes, responds to seasonal changes in climate parameters like temperature and temperature-dependent factors, such as the saturation index of calcite (SIc) and microbial growth (Arp et al., 2001; Gradziński, 2010; Arenas et al., 2014). Arp et al. (2001) showed that in the stromatolites of the creek Deinschwanger, Bavaria, dense small-crystal laminae formed in the summer and autumn months, whereas porous-microspar laminae formed in the winter and spring months. This finding is consistent with the SIc changes in water related to seasonal changes in temperature. Manzo et al. (2012) recognised the succession of spar–microspar–micrite textures in deposits formed over a year in microbial-related tufas in the Corvino Valley, southern Italy.

Therefore, from the aforementioned examples, specifically those referred to natural environments where microbial mats are currently developing, it is plausible to consider that the simple lamina alternations or cycles resulting from texture and porosity variations in ancient laminated microbialites represent 1 year. For Miocene lacustrine stromatolites in the Ebro Basin, cyclic textural and $\delta^{13}C$ and $\delta^{18}O$ variations in the laminae allowed Martin-Bello et al. (2019a, 2019b) to propose an annual duration for each simple couplet, with light porous textures versus dense light and dark textures, corresponding to contrasting precipitation/evaporation ratios. The composite laminae corresponded to multi-annual cycles. Spectral analysis performed by Pérez-Rivarés et al. (2019) on the same stromatolite specimens studied by Martin-Bello et al. (2019a, 2019b) revealed that several periodic to quasi-periodic cycles were recorded. Based on the hypothesis of annual duration for each light and dark lamina couplet, these cycles correspond to 3–7, 8–11 and 22–23-year cycles, and are related to the ENSO and

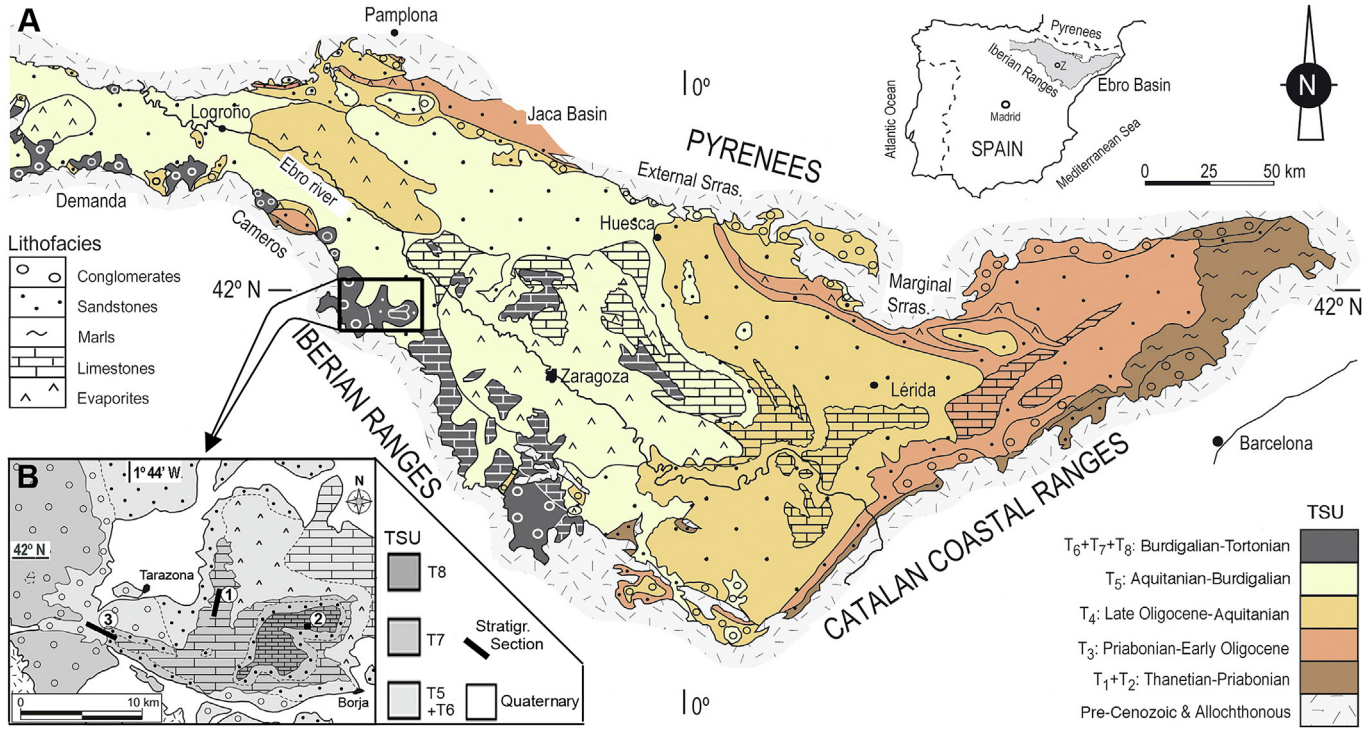

Fig. 1. A) Geological map showing the surface distribution of genetic stratigraphic units and their lithofacies in the Ebro Basin (modified from Muñoz et al., 2002a). B) Map of the Borja–Tarazona sector (modified from Vázquez-Urbez et al., 2013), with the location of stratigraphic sections considered herein. 1: Lugar section; 2: Valdebelengue section; 3: Umbría Alta section. The three sections are represented in Fig. 2. TSU: Tecto-Sedimentary Units.

North Atlantic Oscillation (NAO) precursors, and the Schwabe and Hale cycles, respectively.

Oncolites consist of microbial laminations, which are suitable for the same type of spectral analysis as stromatolites and other laminated deposits. Each light and dark simple lamina couplet resulting from textural and porosity variations can then be hypothesised to represent 1 year, whereas their grouping into light or dark composite laminae would represent multiannual duration intervals (cf. Martin-Bello et al., 2019a). On the basis of this temporal premise, this study: 1) explores whether oncolite lamination records periodic climate oscillations as stromatolites do, 2) correlates the obtained periods with known solar and/or atmospheric parameters that may have influenced the periodic development of the microbial mat, and 3) searches for criteria to confirm or reject the 1-year hypothesis on lamina couplet duration. For this purpose, fluvial and lacustrine oncolite specimens from two Miocene genetic stratigraphic units in the Ebro Basin were selected (Units T7 and T8, Muñoz et al., 2002a). The results of this research are notable for studies searching for high-resolution climatic imprints in past environments and can provide strong support for inferring the temporal significance of microbial lamination.

2. Geological context

2.1. General geology of the Ebro Basin

The Ebro Basin is an Alpine inter-montane basin in the north-eastern Iberian Peninsula, bounded by the Pyrenean, Iberian and Catalan coastal ranges (Fig. 1A). Its sedimentary fill is divided into eight genetic stratigraphic units (Tecto-Sedimentary Units, TSU; cf. Pérez-Rivarés et al., 2018), spanning from the Palaeocene to the Late Miocene (Muñoz et al., 2002a). The basin lost its connection with the Atlantic Ocean approximately 36 Ma ago (Costa et al., 2010), during the Priabonian (i.e.

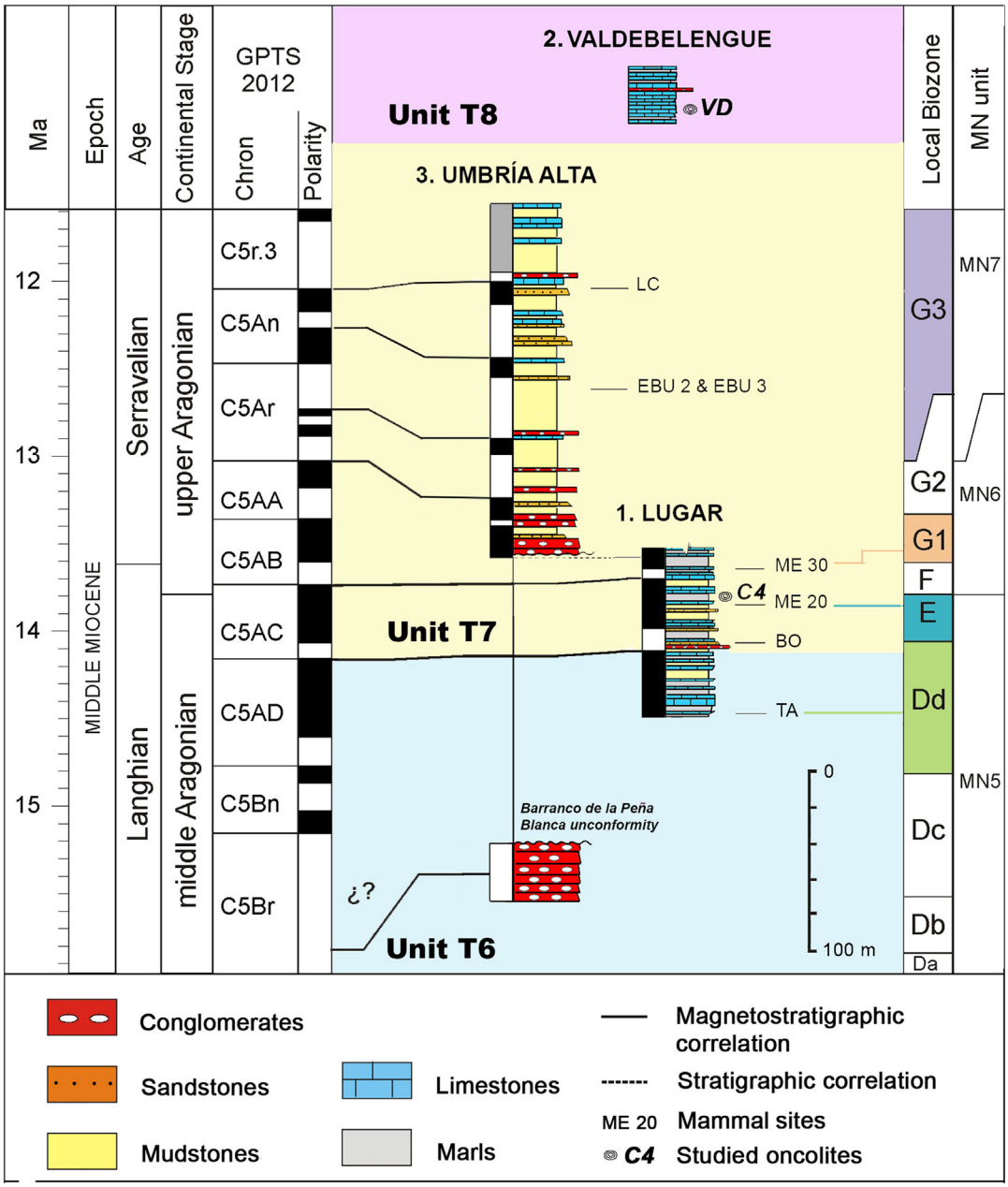

Fig. 2. Stratigraphic sections, summarised from Vázquez-Urbez (2008) and Pérez Rivarés (2016), with magnetostratigraphic dating and the location of micro-mammal sites (from Pérez-Rivarés et al., 2018). The stratigraphic positions of the studied oncolites are presented in sections 1 and 2. Micro-mammal sites: TA: Tarazona de Aragón; BO: Borja; Me: Melero; EBU: El Buste; LC: La Ciesma.

coinciding with the end of the deposition of Unit T2). During the Oligocene and Miocene, only continental deposition existed via alluvial systems, originating from the basin-bounding mountain ranges, and lacustrine systems in the basin centre. Units T3–T7 were deposited within this endorheic context. The latest basin-filling stage (Unit T8) is represented by deposits of alluvial and fluvial–open lacustrine systems, likely concurring with the basin opening to the Mediterranean Sea (Vázquez-Urbez et al., 2013) during the Late Miocene.

2.2. Stratigraphic context of the studied oncolite-bearing beds

The oncolites under study occurred in two geographically close stratigraphic sections representing Units T7 and T8 (Figs. 1B, 2). Biostratigraphic and magnetostratigraphic studies have demonstrated their age. Section 1 (named *Lugar*, Vázquez-Urbez, 2008) comprises 154 m of limestones alternating with marlstones and mudstones; sandstones and conglomerate interbeds occur in the lower third of the section. Fig. 2 shows the lower 92 m, for which magnetostratigraphic analyses are available (from Pérez Rivarés, 2016). Section 2 (named *Valdebelengue*, Vázquez-Urbez, 2008) comprises 32 m of oncolitic limestones, less common bioclastic limestones (e.g. molluscs) and calcite-coated up-growing stem limestones. Rare marlstone and carbonate-clast conglomerate interbeds also occur.

In Unit T7, the oncolite specimens C4-1 and C4-31 are in the same bed of section 1, approximately 2 m above the Melero-20 micro-mammal site and 15 m below the Melero-30 micro-mammal site, which are located within the local biozones E and G1, respectively, according to Murelaga et al. (2008). The magnetostratigraphic analyses performed by Pérez Rivarés (2016) and Pérez-Rivarés et al. (2018) allowed us to date the oncolite-bearing bed at 13.8 My. In Unit T8, specimen VD-13 was collected in a limestone bed, located approximately 9 m from the base of section 2 (Fig. 2). The age of this bed is unknown because the only reference is that the strata of Unit T8 lie concordantly on those of Unit T7 (e.g. section 3 named *Umbría Alta* in Fig. 2; Pérez-Rivarés et al., 2018); thus, Unit T8 is younger than 12 My.

3. Sedimentological characterisation of the oncolite beds

In the study area, oncolites are rare in Unit T7 and common in Unit T8 (Vázquez-Urbez, 2008; Vázquez-Urbez et al., 2013). The shapes of the oncolites are diverse, and depend on the particle morphology acting as nuclei in most specimens. The oncolites are close to spherical grains if the nuclei are sub-rounded particles, regardless of their nature. Spherical oncolites are widespread in Unit T7. However, nuclei formed from long and flat particles, such as plant stems, leaves and shells, produce cylindrical and oblong oncolites, and entire trocospiral gastropods produce conical oncolites. This shape variety is a frequently observed feature of oncolites in Unit T8.

In Unit T7, oncolites occur within a 3.6-m-thick tabular-shaped bed, consisting of floatstones and rudstones with a marl matrix. These oncolites range from millimetres to 12.5 cm, mostly spherical or quasi-spherical in shape (Fig. 3A). These oncolite deposits might have formed in littoral areas far from the direct influence of fluvial channels supplying the lake (Vázquez-Urbez, 2008).

Unit T8 oncolites occur as floatstones and rudstones that constitute tabular and lenticular bodies up to 2 m thick, frequently with irregularly undulating erosional bases. The size of these oncolites varied considerably (millimetres to 15 cm long), with most elongating to a cylindrical shape (Fig. 3B). Calcite-coated phytoclast grains are commonly mixed with oncolites. Oncolite and phytoclast beds show horizontal, planar and trough-cross stratifications (sets up to 1.2 m thick). Together, these structures are interpreted to have been formed by the accretion of longitudinal bars, the migration of transverse bars and the filling of low-sinuosity fluvial channels. Although rare, oncolite beds are also arranged as sigmoidal bodies interpreted as point- and as mouth-bar deposits; the latter were produced from fluvial channels entering shallow lake areas. In brief, oncolite beds of Unit T8 were formed by deposition in shallow fluvial channels and shallow marginal lake areas subjected to agitation (Vázquez-Urbez et al., 2013).

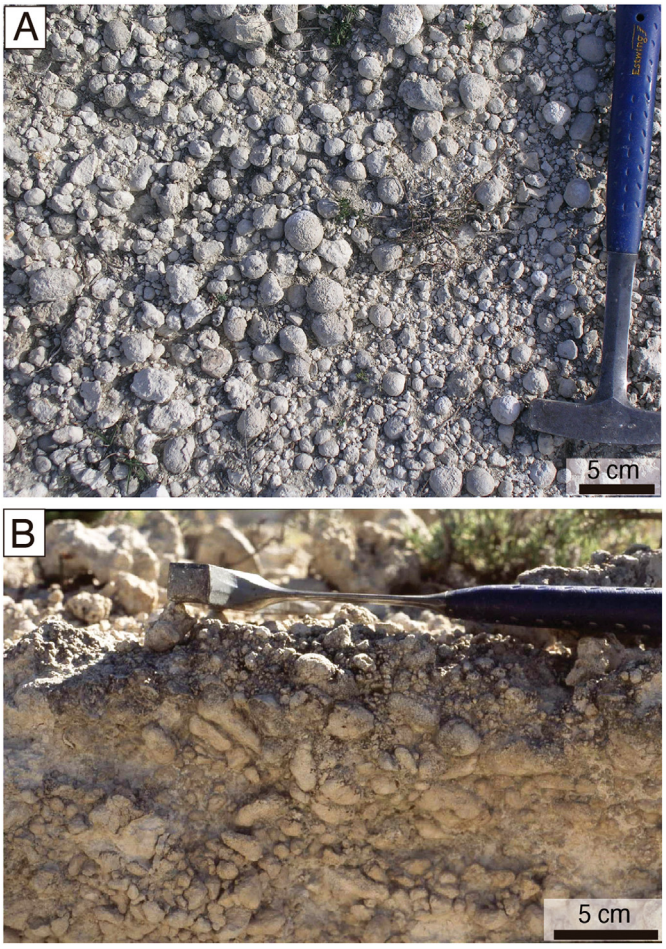

Fig. 3. Field views of two oncolitic layers studied in this work: A) Mostly spherical oncolites in Unit T7 (plan view). B) Oncolites of various shapes in Unit T8 (base to top view).

4. Materials and methods

Three oncolite specimens were selected primarily based on the thickness of the laminated coatings and the greatest number of laminae: two in Unit T7 (C4-1 and C4-31) and one in Unit T8 (VD-13). The continuous character of lamination, the lamina distinction and the small volume of porosity were also crucial for specimen selection. The macroscopic and microscopic characteristics of these specimens are described in the following section.

Several cross-sections were made across the three specimens. High-resolution images (HRI, 1200 ppi) were obtained by digitally scanning the polished sections across the lamination (Fig. 4). One-half was used to obtain thin sections for textural and structural studies using optical microscopy on each specimen. Thin sections were prepared at the *Servicios de Apoyo a la Investigación* (SAI) of the University of Zaragoza, Spain. Observations and images were obtained using a petrographic polarised light microscope (Olympus AX-70) and a digital photography camera (Olympus E-330) of the SAI. The other half was used for lamina thickness and raw pixel luminance measurements, and sampling for stable isotope analyses of C and O in specimen C4-31.

In the polished cross-sections, the oncolites contain simple alternating lamination (as defined by Monty, 1976) that can be observed at different scales. Herein, a simple lamina is considered 'the smallest

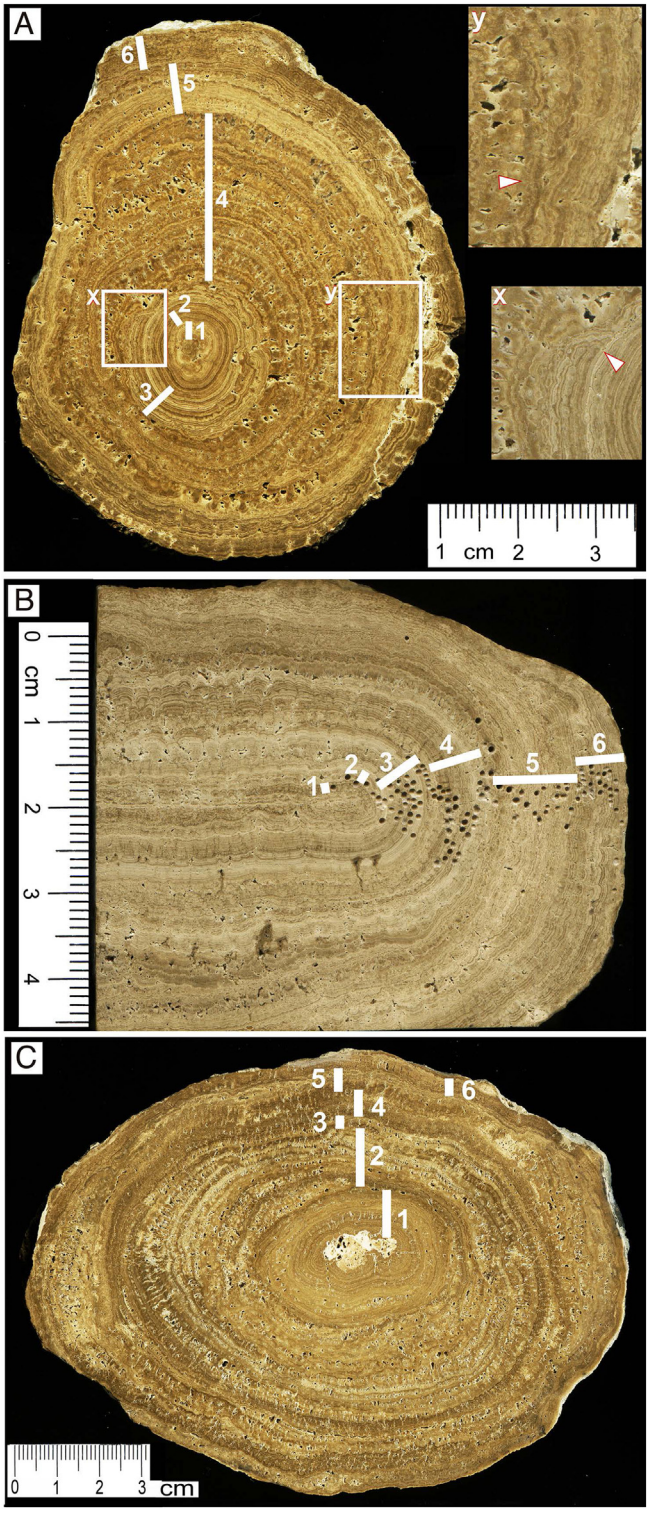

Fig. 4. Images of scanned sections of the oncolites under study. The white bars perpendicular to the lamination indicate the segments through which thickness measurements of simple laminae were run. A) Oncolite C4-1 developed on a nucleus consisting of grouped millimetre-long oncolites. The lamina shape and discontinuity details are shown in windows x and y (arrowed). B) Oncolite C4-31 grew on a leaf 5.5 cm long and >12.5 cm wide. C) Oncolite VD-13 nucleated on an irregular angular calcareous clast 1.8 cm × 1 cm in size.

layering unit' with uniform texture, following Walter (1972) and Arenas and Jones (2017). Different textures are manifested through colour tone variations: darkness and light. These simple laminae were the target of thickness measurements for subsequent periodicity analysis. Groups of dark and light simple laminae produced dark and light composite laminae, each formed of a dominant lamina type.

The lamina thickness was manually delimited; divisions representing every lamina thickness were traced across the specimens (Fig. 5). The thickness of these divisions was measured by the multi-purpose software for stratigraphic signal analysis called Strati-Signal (Ndiaye et al., 2012). Raw pixel luminance values (between 0 = black and 100 = white) were obtained directly from HRI in the CIE-L*a*b* colour space through the same segments used for lamina thickness measurements and using the same multi-purpose software. A more detailed explanation of the data acquisition is included in the Supplementary material. The lamina thickness, raw luminance and stable isotope values acquired from the polished sections were used to analyse the periodic signal of the oncolite lamination (Supplementary material and Table S1).

4.1. Selecting sampling segments for lamina thickness and raw luminance measurements

Owing to the discontinuous character of some laminae (Fig. 4A) and to avoid artefacts or defects, running several segments was necessary to cover every specimen fully. Thus, thickness measurements were performed through several segments perpendicular to the lamination that were selected on HRI of the cross-sections of specimens, searching for the maximum neatness of the simple laminae, the best correlation between successive segments and spanning the maximum number of laminae with no discontinuities between them (Fig. 4). For each specimen, the sum of several segments spanning the entire laminated coating produced a single succession of simple lamina thicknesses. In specimen C4-31, sampling for stable isotope analysis was performed close to and coinciding with the path of the six segments used for simple lamina thickness and luminance measurements (Fig. 4B).

The most challenging task concerned simple lamina thickness measurements of some segments formed of poorly differentiated laminae, typically observed with high porosity. Their thickness values may not be accurate and could introduce errors in calculating other parameters relying on them (e.g. the time represented by or the growth rate of lamination) or alter the spectral analysis results.

4.2. $\delta^{13}C$ and $\delta^{18}O$ analyses

A cross-section of specimen C4-31 correlative to the luminance and thickness measurement sections was sampled using a 0.5 mm diameter micro-drill powered by a micro-motor (Navfram model N120 Micro-

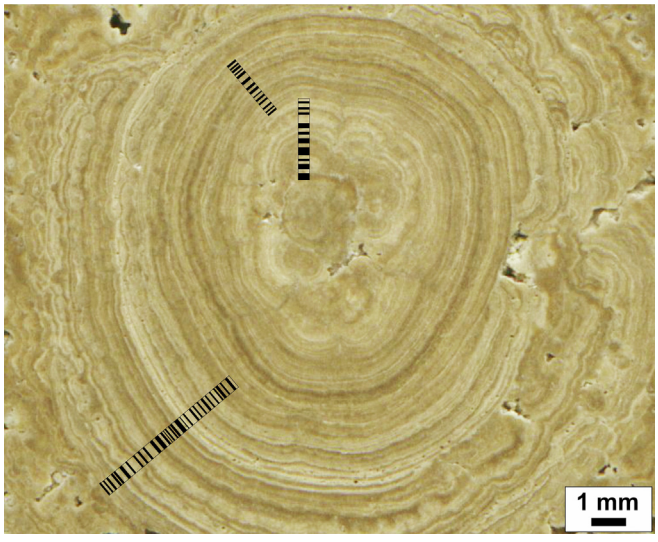

Fig. 5. Example of recognition and thickness measurement of simple light and dark laminae used in spectral analysis (sample C4-1).

motor 25.000 rpm with an electronic speed regulator, AB SHOT TECNICS SL, Cervello, Barcelona, Spain). The device was coupled with a stereo microscope, which helped select the rock parts with the minimum cements or recrystallisation features (as was also determined in the thin sections). Acquiring as many samples as possible at the closest possible intervals yielded 43 rock powder samples through a 3.2-cm-long path (Fig. 4B). Each sample spanned 3–13 simple laminae grouped into light and dark intervals. Powdered samples (0.2–0.5 mg) were stored in glass vials. All analysed samples were formed of calcite (as determined by the petrographic features of thin sections and correlative alizarine red-dyed parts).

The $\delta^{13}C$ and $\delta^{18}O$ ratios were determined using a mass spectrometer (MAT-252, Thermo Finnigan; Thermo Fisher Scientific, Waltham, MA, USA) at the Servicios Científico-Técnicos (CCIT-UB Serveis) of the University of Barcelona, Spain. The values were measured via CO_2 obtained in a Carbonate Kiel Device III (Thermo Finnigan) by reacting samples with 100 % H_3PO_4 at 70 °C for 3 min (McCrea, 1950). The international standards NBS-19 ($\delta^{13}C$ V-PDB = +1.95 ‰ and $\delta^{18}O$ V-PDB= −2.20 ‰) were used to calibrate $\delta^{13}C$ and $\delta^{18}O$ to the Vienna Pee-Dee Belemnite (V-PDB). The results are reported in ‰ relative to V-PDB. The overall reproducibility was better than 0.02 ‰ for $\delta^{13}C$ and 0.04 for $\delta^{18}O$. The values of $\delta^{13}C$ and $\delta^{18}O$ (Table 1) were used for the sedimentological interpretation and periodicity analysis.

Regarding the influence of diagenetic features on diverse measurements and analyses, all samples were examined under an optical microscope to select the most pristine zones, where dissolution and replacement features were absent or minimal. Most cavities were empty in specimens C4-1 and C4-31. However, specimen VD-13 contained more calcite cement-filling pores than the other specimens. This type of post-sedimentary feature was avoided in the thickness and luminance measurements and rock sampling for stable isotope analysis.

Table 1
Stable isotope values ($\delta^{18}O$‰ V-PDB and $\delta^{13}C$‰ V-PDB) of consecutive calcite samples obtained in oncolite C4-31.

Sample	$\delta^{13}C$ (V-PDB)	$\delta^{18}O$ (V-PDB)
C4-31-1	−7.25	−8.89
C4-31-2	−7.30	−8.82
C4-31-3	−7.64	−8.72
C4-31-4	−7.63	−8.86
C4-31-5	−7.44	−9.10
C4-31-6	−7.37	−8.93
C4-31-7	−7.60	−8.84
C4-31-8	−7.43	−8.85
C4-31-9	−7.56	−8.89
C4-31-10	−7.69	−8.81
C4-31-11	−7.81	−8.85
C4-31-12	−7.58	−8.96
C4-31-13	−7.45	−8.59
C4-31-14	−7.52	−8.91
C4-31-15	−7.31	−8.91
C4-31-16	−7.28	−8.76
C4-31-17	−7.29	−8.85
C4-31-18	−7.18	−8.72
C4-31-19	−7.29	−8.74
C4-31-20	−7.33	−8.86
C4-31-21	−7.60	−8.86
C4-31-22	−7.47	−8.86
C4-31-23	−7.56	−8.89
C4-31-24	−7.39	−9.01
C4-31-25	−7.43	−9.09
C4-31-26	−7.55	−9.14
C4-31-27	−7.49	−9.16
C4-31-28	−7.40	−9.07
C4-31-29	−7.46	−9.17
C4-31-30	−7.52	−8.98
C4-31-31	−7.36	−9.05
C4-31-32	−7.43	−9.08
C4-31-33	−7.74	−8.91
C4-31-34	−7.75	−9.11
C4-31-35	−7.78	−9.06
C4-31-36	−7.58	−9.05
C4-31-37	−7.75	−8.92
C4-31-38	−7.69	−8.83
C4-31-39	−7.44	−8.87
C4-31-40	−7.39	−8.85
C4-31-41	−7.46	−8.89
C4-31-42	−7.24	−9.04
C4-31-43	−7.44	−9.0

4.3. Periodicity analysis

Many time-series have been generated with lamina thickness, raw pixel luminance and isotope data. Spectral analysis was implemented using the ACYCLE time-series software (Li et al., 2019). To avoid power leakage from very low-frequency components to higher frequencies of the spectrum (Kodama and Hinnov, 2015), we removed long-term secular trends using locally estimated scatterplot smoothing (LOESS). A 35 % window size was applied for a good data fit, removing the power spectrum of the lower frequencies, which are more affected by the background of red noise. It has been necessary to perform this method in order to improve the isolation of the spectral peaks, due to the low number of cycles available from the oncolites and the complexity of the lamination. The multi-taper (MTM; Thomson, 1982) and smoothed periodogram methods (MatLab's periodogram) were applied to power spectral analysis. A 2π MTM with five zero-padding cycles was used. In the periodogram method, the time-bandwidth = 2.

To test the significance of the spectral peaks against the background of the power spectrum, we applied a first-order autoregressive model AR(1) (RedNoise.m, Husson, 2014, modified by Linda Hinnov, Li et al., 2019) to form a theoretical red noise spectrum and false alarm with confidence levels of 90 %, 95 % and 99 % (Thomson, 1990). The 90 % and 95 % confidence levels were applied to evaluate false negatives because several factors could mask the solar signal isolation in the laminae thickness variations. A 20 % moving average window was applied.

Wavelet analyses were also performed (Torrence and Compo, 1998). A Morlet wavelet base (wavenumber: 6) was used. The time series was padded with zeros at both ends to limit the edge effect. The statistical significance of the wavelet power spectrum is expressed using a cone of influence generated with AR(1) with a confidence threshold of 95 %.

5. Results

5.1. Characteristics of the oncolite laminae and lamination

The texture and structure of the oncolites in Units T7 and T8 have been described by Vázquez-Urbez (2008) and Vázquez-Urbez et al. (2013). This paper includes such results and some new data gathered through this research, as contextual information to help interpret lamina cyclicity within the depositional context and the results derived from the periodicity analyses performed herein.

In polished cross-sections, the oncolites consist of alternating light and dark calcite laminae concentrically arranged around the nuclei. The light laminae are cream, light brown and light grey; the dark laminae are brown and grey. The laminae are either continuous and isopachous throughout the coating or present lateral variations in thickness (Fig. 6A) up to their disappearance in some parts of the coating (Fig. 4A).

The thickness of the simple lamina couplets varies between 78 and 607 μm/couplet depending on the segment (Table 2). The average values are 205 and 243 μm/couplet in Unit T7 oncolites and 259 μm/couplet in the Unit T8 oncolite. These values do not include composite laminae or lamina intervals with disorganised and massive characteristics (i.e. segment 4 in oncolite C4-1 and segment 2 in oncolite VD-13; Fig. 4A, C).

In optical microscope views, lamination is composed of alternating dense dark micrite laminae and dense or porous light microspar to spar laminae (Figs. 6B and C, 7A and B). The thickness of the laminae ranges from a few tens of microns to a few hundreds of microns, and varies through the cortices and specimens. These simple laminae are grouped into composite laminae wherein micrite or microspar textures

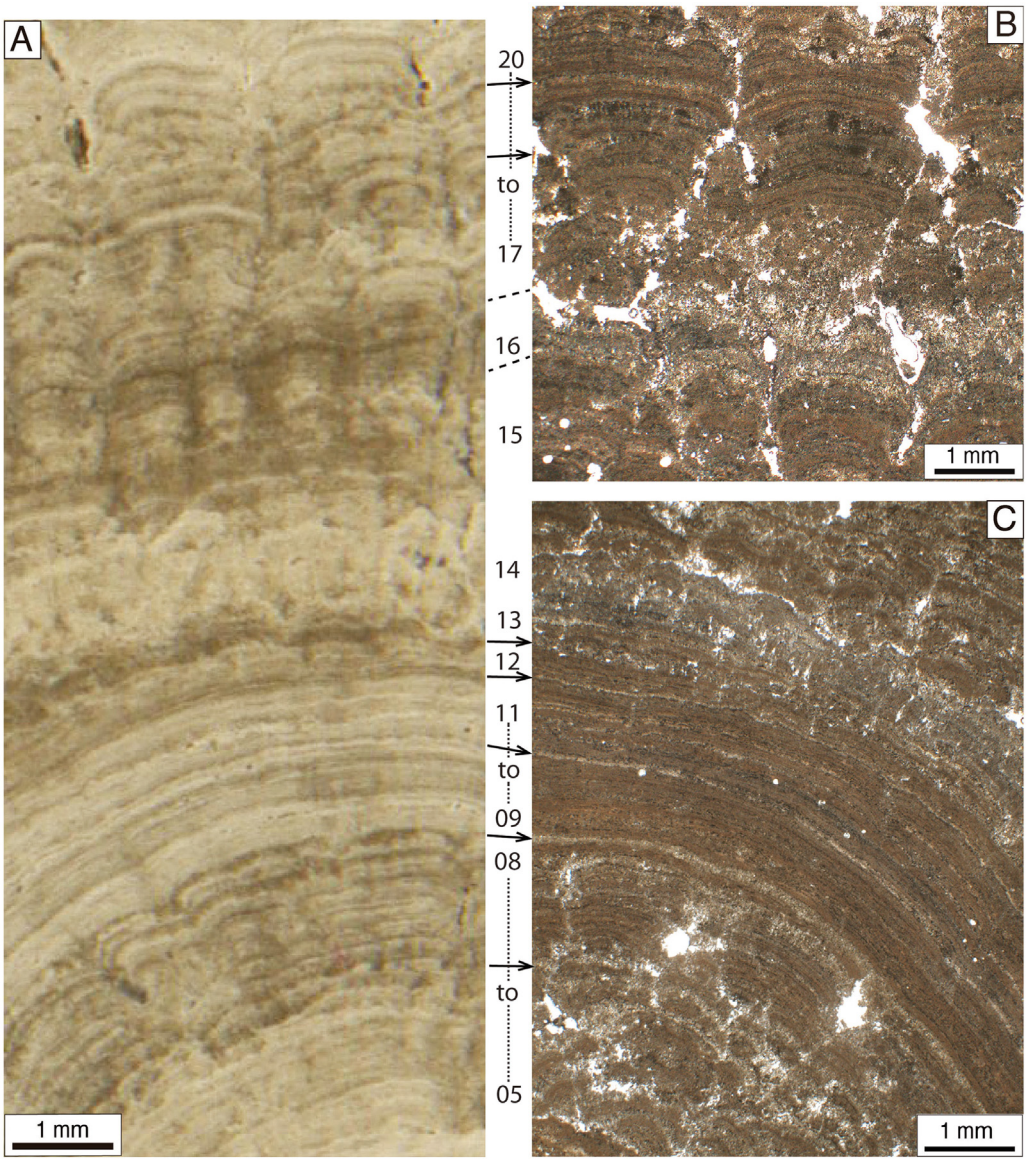

Fig. 6. Images of the oncolite C4-31. A) Polished slab sample. B) and C) Photomicrographs (optical microscope, plane-polarised light) corresponding to close areas of the image in A. The numbers in the central column correspond to the intervals sampled for stable isotope analyses (Figs. 8, 9). The arrows indicate the equivalence between laminae in the polished and microscope views.

dominate, and commonly are distinguished by colour tone variations (Figs. 6B and C, 7A and B). Thick, porous intervals consisting of poorly differentiated laminae are formed primarily of micrite and microspar calcite (e.g. lamina 14 shown in Fig. 6). These intervals are not a standard feature.

Table 2
Thickness data and averaged measures (in μm) in the three oncolites.

	Light–dark	Light	Dark
C4-31			
Mean	205	84	120
Max	465	233	336
Min	78	26	52
C4-1[a]			
Mean	243	107	136
Max	607	354	405
Min	101	25	51
VD-13[b]			
Mean	259	109	150
Max	593	495	415
Min	99	20	59

[a] Without segment 4 (Fig. 4A).
[b] Without segment 2 (Fig. 4C).

The correspondence of the light–dark colours between the polished samples and the microscope observations depends on porosity and crystal size. Either simple or composite, the light-coloured laminae in the polished sample correspond to dense dark micrite laminae in microscopic views (Fig. 6A, B and C). The dark-coloured laminae in the polished sample correspond to dense or porous light microspar to spar laminae in microscopic views (e.g. laminae 15 and 16 shown in Fig. 6). These are the dominant features, although exceptions exist.

The boundaries between the simple laminae are either sharp or gradual. Gradual boundaries are seen from microspar to micrite laminae, and sharp boundaries are seen from dark micrite to microspar or spar laminae. Either simple or composite, the laminae are smooth, undulate, festooned and domed in shape. The lamina shape (2D sections) can vary from base to top through a composite lamina and laterally within the same lamina. In several cases, smooth and slightly undulating continuous laminae are dominant close to the oncolite nucleus (e.g. in specimen C4-1; Fig. 4A). In other cases, the smooth laminae form flat intervals that alternate with dominantly domed lamina intervals, both spanning several composite laminae groups (e.g. in specimen

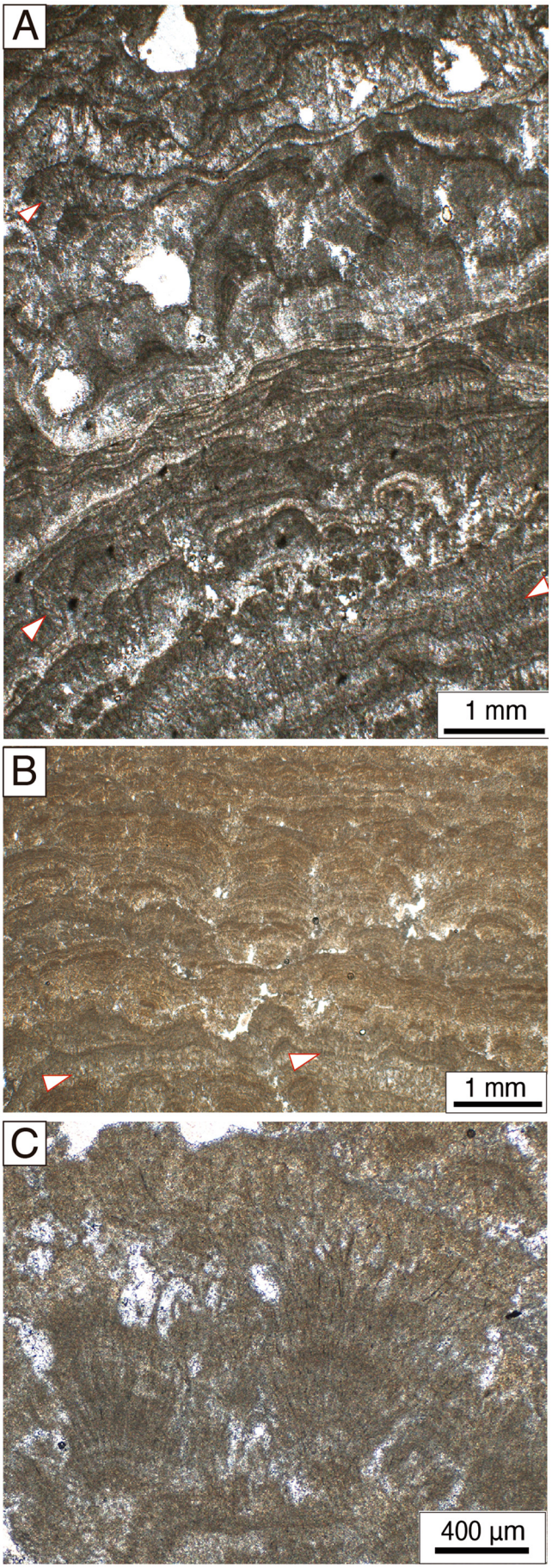

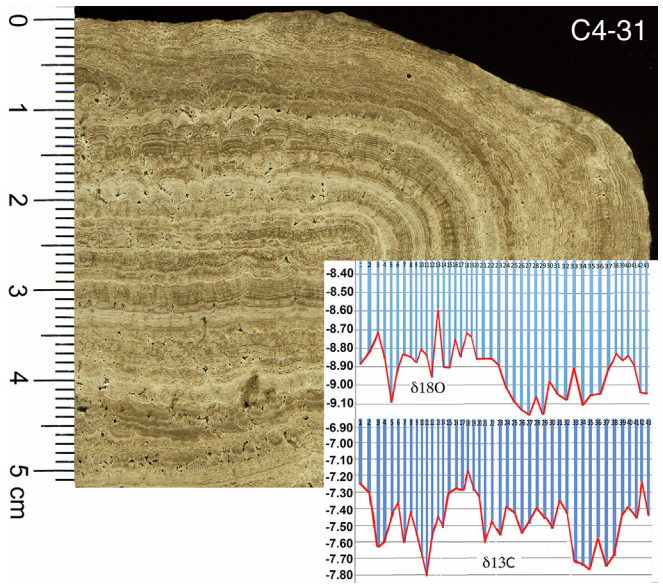

Fig. 8. Image of the oncolite C4-31 cross-section with stable isotope values ($\delta^{13}C$ and $\delta^{18}O$, ‰ V-PDB) through the segment sampled for isotopic analyses.

C4-31; Fig. 4B). Some other intervals are characterised by irregular and discontinuous laminae, challenging lamina recognition (e.g. in specimen VD-13; Figs. 4C, 7A).

These poorly laminated intervals sometimes have high interparticle and frame-growth porosities coinciding with columnar and domed structures (e.g. in specimen C4-31; Fig. 6). The domed and columnar intervals contain higher porosity, i.e., irregular pores between domes and columns, owing to animal bioturbation (Fig. 6). The pores are empty and irregular in shape and size, and vertical to sub-vertical pores are common, reaching up to 4 mm long. The latter cavities dominate the inter-dome and inter-columnar spaces. Elongated pores are better developed in specimen VD-13 than in the other specimens.

Micrite and microspar filament-shaped bodies that are 50–400 μm in length and 7–15 μm in diameter were observed in some laminae. These filaments are attributable to bacterial bodies, likely cyanobacterial bodies. They can be loosely arranged filaments forming fences or palisades, frequently observed in the continuous and smooth laminae (lower parts of Fig. 7A and B). In other cases, the filaments are radially arranged, forming isolated or, more commonly, adjacent fan-shaped structures, which frequently constitute discontinuous laminae, particularly those with domed and columnar growth (upper parts of Fig. 7A and C).

5.2. $\delta^{13}C$ and $\delta^{18}O$ composition

The C4-31 specimen yielded $\delta^{13}C$ values between −7.24 ‰ and −7.81 ‰, with a mean of −7.49 ‰ V-PDB. The $\delta^{18}O$ values ranged between −8.72 ‰ and −9.17 ‰, with a mean of −8.93 ‰ V-PDB (Table 1). No correlation existed between $\delta^{13}C$ and $\delta^{18}O$ ($r = 0.08$; $N = 43$). Each stable isotope value represents 3–13 simple laminae wherein either light or dark laminae were dominant (Figs. 4B, 6A). There is no evident pattern of isotopic variation in the values of the light and dark lamina dominant groups of C or O (Fig. 8). The mean $\delta^{13}C$ and $\delta^{18}O$ values were more negative in the light groups than in the dark groups (polished sample), with differences of 0.12 $\delta^{13}C$ and

Fig. 7. Photomicrographs (optical microscope, plane-polarised light) of the studied oncolites. A) Wavy and domed lamination in oncolite VD-13. Note the high porosity and abundance of cyanobacterial micrite filaments grouped into fan- and shrub-shaped bodies (arrowed). B) Gently domed lamination in oncolite C4-1. Cyanobacterial micrite filaments sub-perpendicular to laminae occur loosely and grouped in palisades (arrowed). C) Detail of radially arranged cyanobacterial filaments.

0.10 $\delta^{18}O$. The least negative values of both isotopes coincided approximately between samples 13 and 19, and the $\delta^{18}O$ values tend towards increasingly negative values over time (Figs. 8, 9).

5.3. Spectral analysis

The time-series spectral analysis based on the lamina thicknesses and raw luminance of the three studied oncolites (Supplementary material) allowed for the recognition of periodic or quasi-periodic components through lamination. Several statistically significant power spectrum peaks (hereafter, spectral peaks) were revealed in the multitaper (MTM) spectra of specimens C4-31, C4-1 and VD-13; the three specimens share several significant peaks within the same frequency bands (Figs. 10–13). The spectral analysis of light and dark laminae separately yielded results that were not significantly different from those obtained by the spectral analysis of the light–dark couplets. The spectral results are shown in Supplementary material. Smoothed periodograms are presented also in Supplementary material.

5.3.1. Oncolite C4-31

The MTM spectral analysis of the light–dark lamina couplet thickness of specimen C4-31 (Fig. 10A) revealed several statistically significant periods: a spectral peak of approximately 11 couplets (10.9), a double peak with values of 18.7 and 21.4 and another peak at 2.4 (above the 99 % confidence level). Other relevant peaks arise around 5.9 and 2.8, exceeding the 95 % confidence level. The wavelet spectra of the raw luminance (Fig. 10C) show that part of the oncolite (between couplets 77 and 90) does not reflect properly the period 11. However, the elimination of the worst defined interval is not feasible due to the limited data number. In contrast, the period around 22 is widely represented all through the oncolite. The MTM spectrum of the raw luminance data (Fig. 10B) shows several significant peaks at the 2.5–3.4 period band. At frequencies lower than that, two peaks arise around period 5.8 (exceeding the 95 % confidence level), and another peak that almost reaches 99 % occurs at period 19.9. A peak was observed at period 9.7, but did not reach the 90 % confidence level.

The MTM spectral analysis based on the stable isotope data obtained from specimen C4-31 (Fig. 11) shows results consistent with the lowest frequency spectra yielded by the lamina thickness. For $\delta^{18}O$ (Fig. 11A), significant spectral peaks are clustered around two frequency bands: the most significant peak appears at period 20.9 (above the 99 % confidence level). A double peak occurs around 11, with a >95 % confidence level, and a third peak above 95 % emerges at 9.2. For $\delta^{13}C$ (Fig. 11B), significant power spectrum values are repeated around 22.9 and 13.3.

5.3.2. Oncolite C4-1

The MTM spectral analysis of the light–dark lamina couplet thickness of specimen C4-1 (Fig. 12A) allowed the detection of significant periodicities above the 95 % confidence level around 11, 4.2 and 2.4 (with 99 % in the case of the 4.2 peak). Notably, a peak occurs at 20.2, which is above the 90 % but does not reach the 95 % confidence level.

The pixel-luminance data spectrum (Fig. 12B) shows numerous significant peaks (over the 99 % confidence level) in the frequency band between 0.3 and 0.5, equivalent to periods 3.1 to 2.1. At frequencies

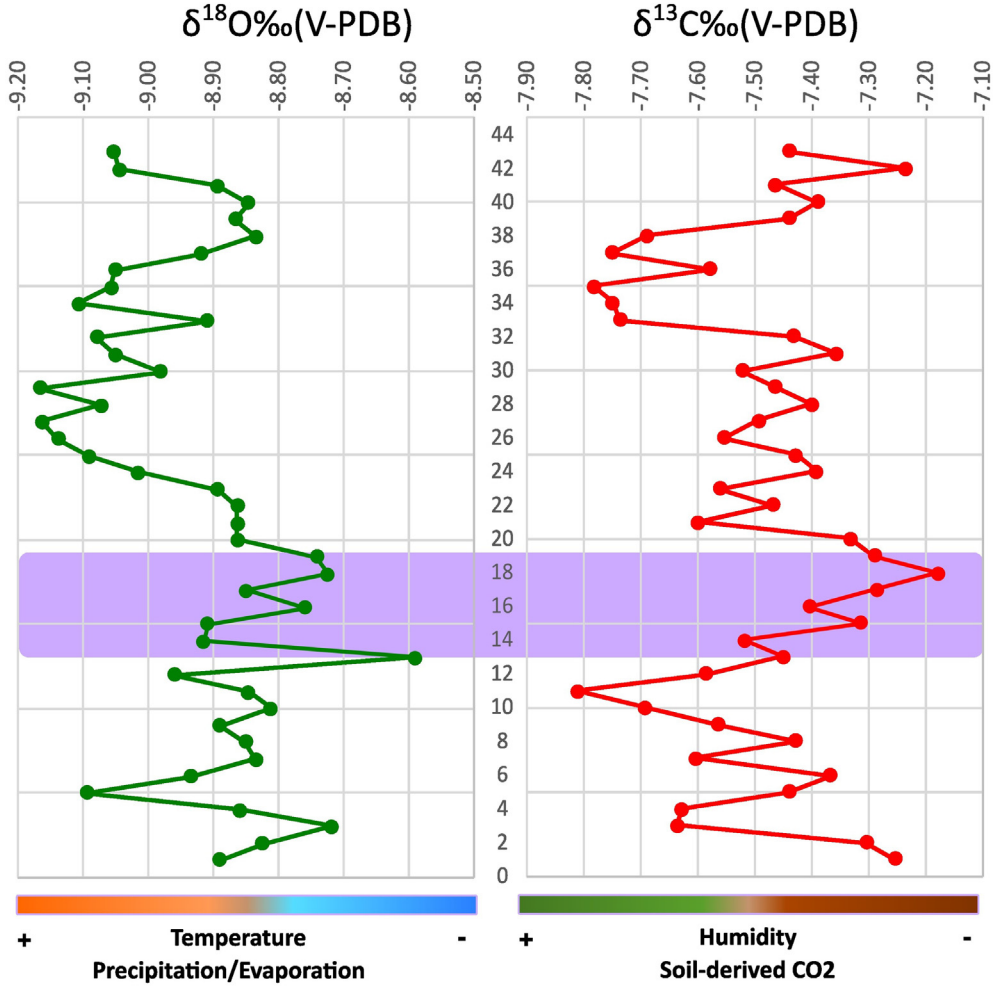

Fig. 9. Plot of stable isotope variations ($\delta^{13}C$ and $\delta^{18}O$, ‰ V-PDB) through oncolite C4-31. Note the least negative values of samples 13–19 (highlighted in purple). The vertical axis corresponds to the sampling points from the nucleus outwards.

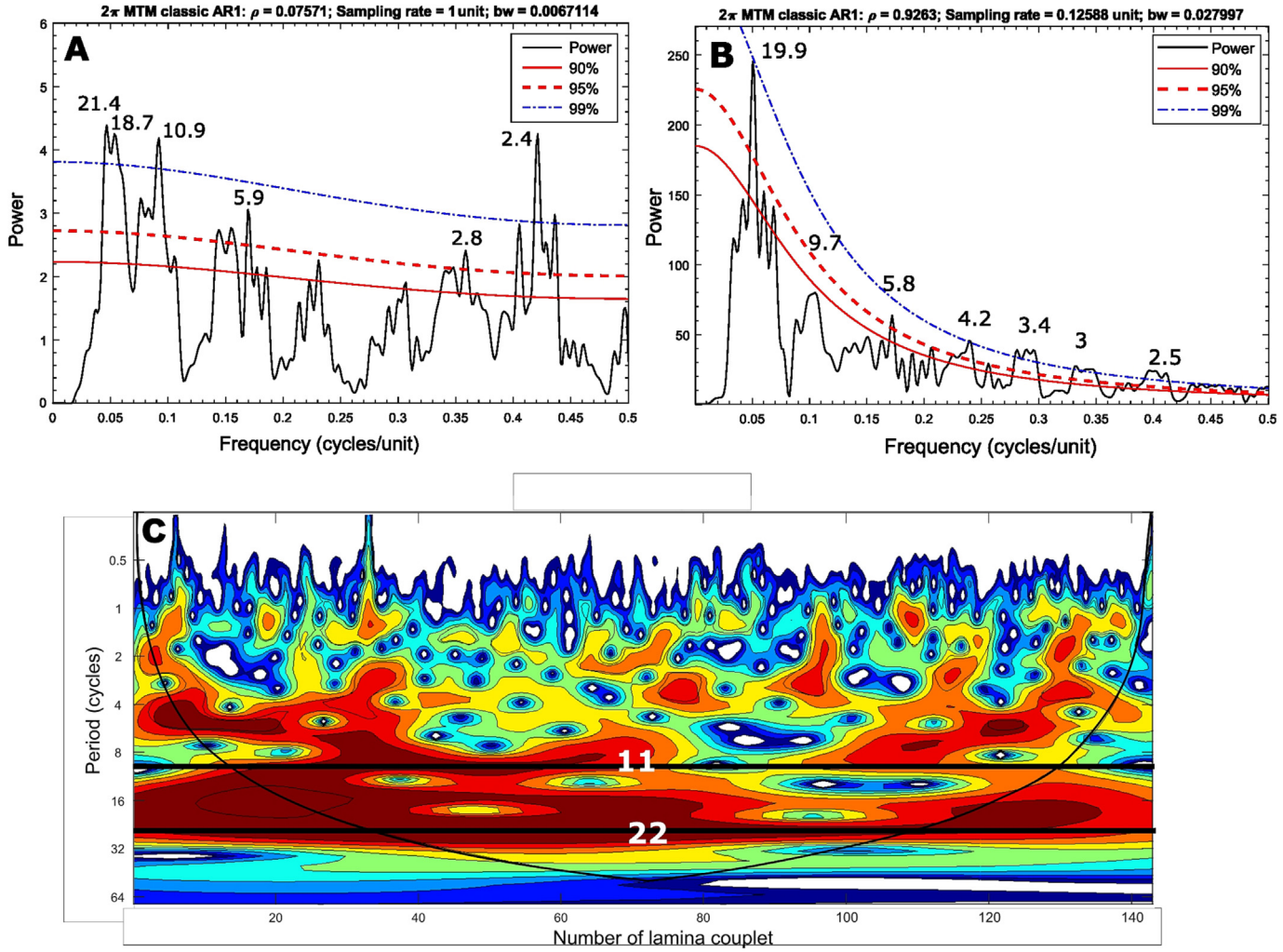

Fig. 10. Representative spectral and continuous wavelet analyses of specimen C4-31: A) 2π MTM power spectrum and B) periodogram from the thickness of lamina couplets; C) 2π MTM power spectrum from isolated dark and D) light (down) lamina thickness; E) wavelet spectrum from the thickness of lamina couplets; F) 2π MTM power spectrum from raw luminance data obtained from the same thickness measurement segments as in A. The coloured lines in the power spectrum graphs represent standard confidence levels for rejecting the null AR (1) red noise, null hypothesis models with a 20 % median filter length and linear fitting. The thick black contour in the wavelet spectrum indicates the 95 % confidence level, and the region below the thin line indicates the cone of influence. The term "units" corresponds to the time interval represented by a couplet formed of a dark lamina plus a light lamina.

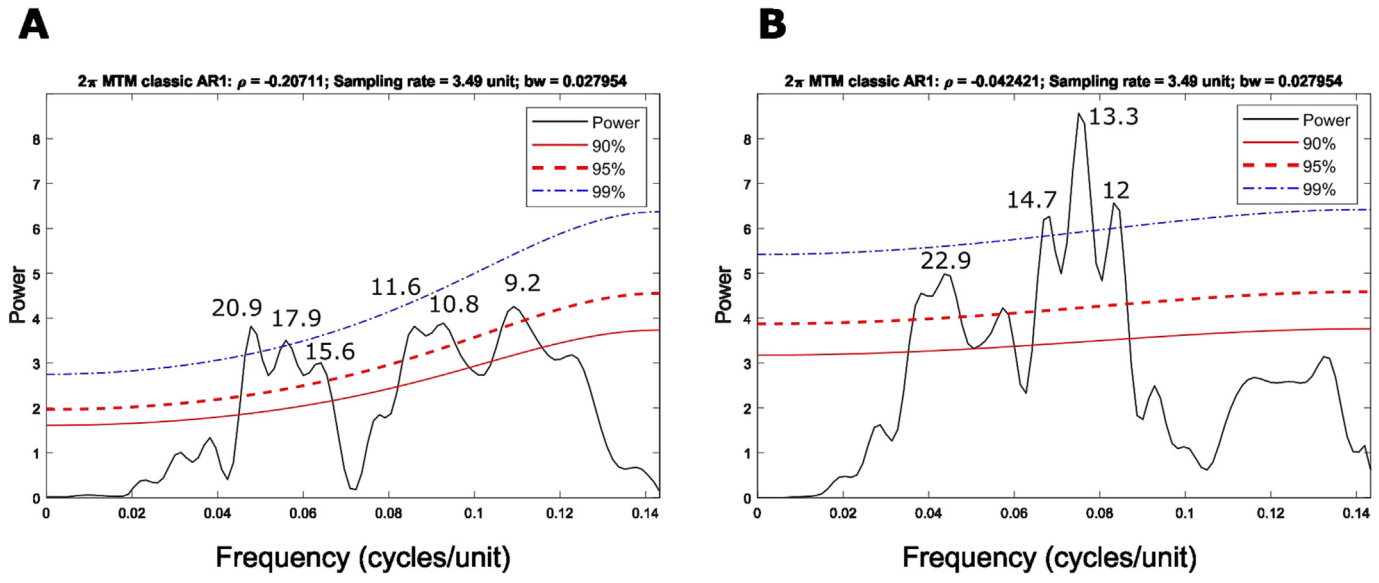

Fig. 11. 2π MTM power spectrum from stable isotope data of specimen C4-31: A) $\delta^{18}O‰$ V-PDB; B) $\delta^{13}C‰$ V-PDB.

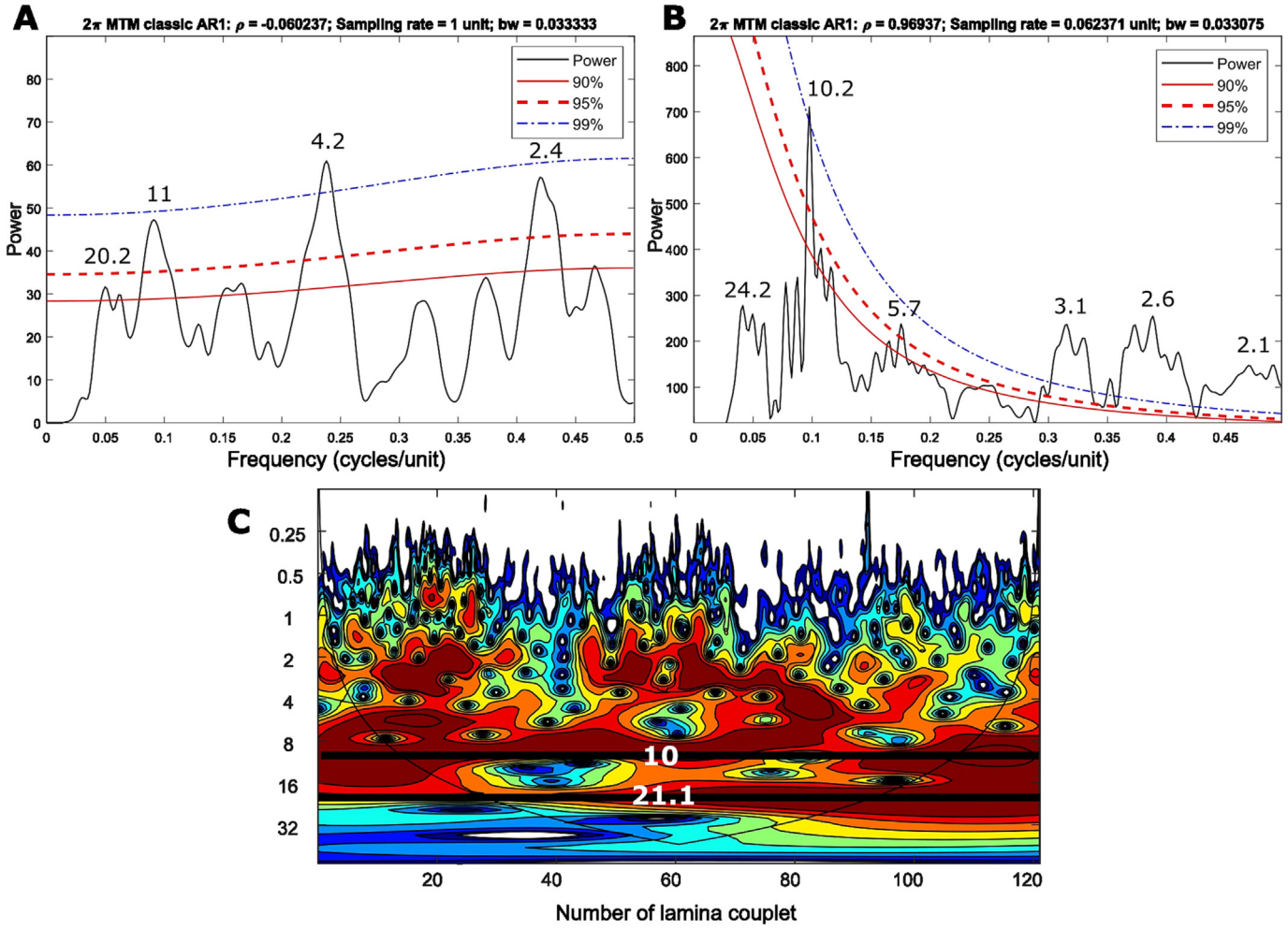

Fig. 12. Representative spectral and continuous wavelet analyses of specimen C4-1: A) 2π MTM power spectrum from the thickness of lamina couplets; B) 2π MTM power spectrum from raw luminance data of the same thickness measurement segments as in A; C) wavelet spectrum from raw luminance data. The term "units" corresponds to the time interval represented by a couplet formed of a dark lamina plus a light lamina.

lower than that, only two peaks exceed the 95 % confidence level: at periods of 10.2 (over 99 %) and 5.7. The peak at 24.2 does not reach the 90 % confidence level. The wavelet analysis performed on the luminance data (Fig. 12C) indicates two preferred periods showing high continuity throughout the sample at approximately 21.1 and 10.

5.3.3. Oncolite VD-13

Specimen VD-13 has textural characteristics that make the spectral analysis particularly problematic. This specimen presents intervals of poorly differentiated lamination, typically with high porosity and the lamina thickness is highly variable. Therefore, some of the measured thickness values might not correspond to the actual simple lamina thickness, which could alter the spectral analysis results. Thus, in oncolite VD-13, two series of analyses were performed to evaluate differences because of problematic segments: one including all the measurable laminae of the oncolite (VD-13A) and one excluding the most problematic segment (VD-13B), e.g. segment 2 (Fig. 4C).

The MTM analysis based on the thickness of all light–dark lamina couplets of VD-13A (Fig. 13A) presents a group of spectral peaks in the frequency band between 0.05 and 0.1, with a dominant peak at period 13.2, exceeding the 99 % confidence level, and another peak at period 9.7. Three other peaks reach or exceed the 95 % confidence level at periods 7.1, 4.2 and 2.5. Wavelet analysis (Fig. 13B) shows some continuity in periods close to 11 and 22, which tend to disappear at the lower part of the specimen, below datum 60.

Due to the limited data number, the exclusion of all problematic intervals is not feasible. After removing the segment 2 values, the spectral analysis of VD-13 (i.e., VD-13B) through the MTM based on light plus dark lamina couplets (Fig. 13C) detected an isolated peak around period 11.9, reflected in the VD-13A spectrum as a double peak. The peaks around periods 7, 4.2, 3 and 2.4 are still present.

Thus, by eliminating the segment 2 values of specimen VD-13 in the analysis (Fig. 13C), a couplet spectrum with better-defined frequencies around 0.09 is obtained, and the spectral peak corresponding to this frequency increases its confidence level. Moreover, the spectrum continuity is greatest in the wavelet analysis at frequencies around period 11 (Fig. 13D).

The results obtained from the spectral analysis performed on the raw luminance data of VD-13A (Fig. 13E) resemble those based on the thickness data (Fig. 13A); i.e. the primary significant spectral peaks of both data types happen at similar frequency positions: periods 13.4, 11.8, 8.5, 4.8 and 2.8. Wavelet analysis shows the greatest continuity at periods 12.3 and 22.6 (Fig. 13F). Once segment 2 was deleted from the time-series, the MTM analysis showed highly significant peaks in periods slightly lower than the aforementioned ones (Fig. 13G) and highlighted a distinctive double peak between 10.2 and 12.6. In the wavelet analysis (Fig. 13H) the latter peak manifests with substantial continuity around period 11.3. In addition, the period around 22.6 reduces the significance level with respect to the wavelet analysis of VD-13A (Fig. 13F). Therefore, the elimination of segment 2 reduces

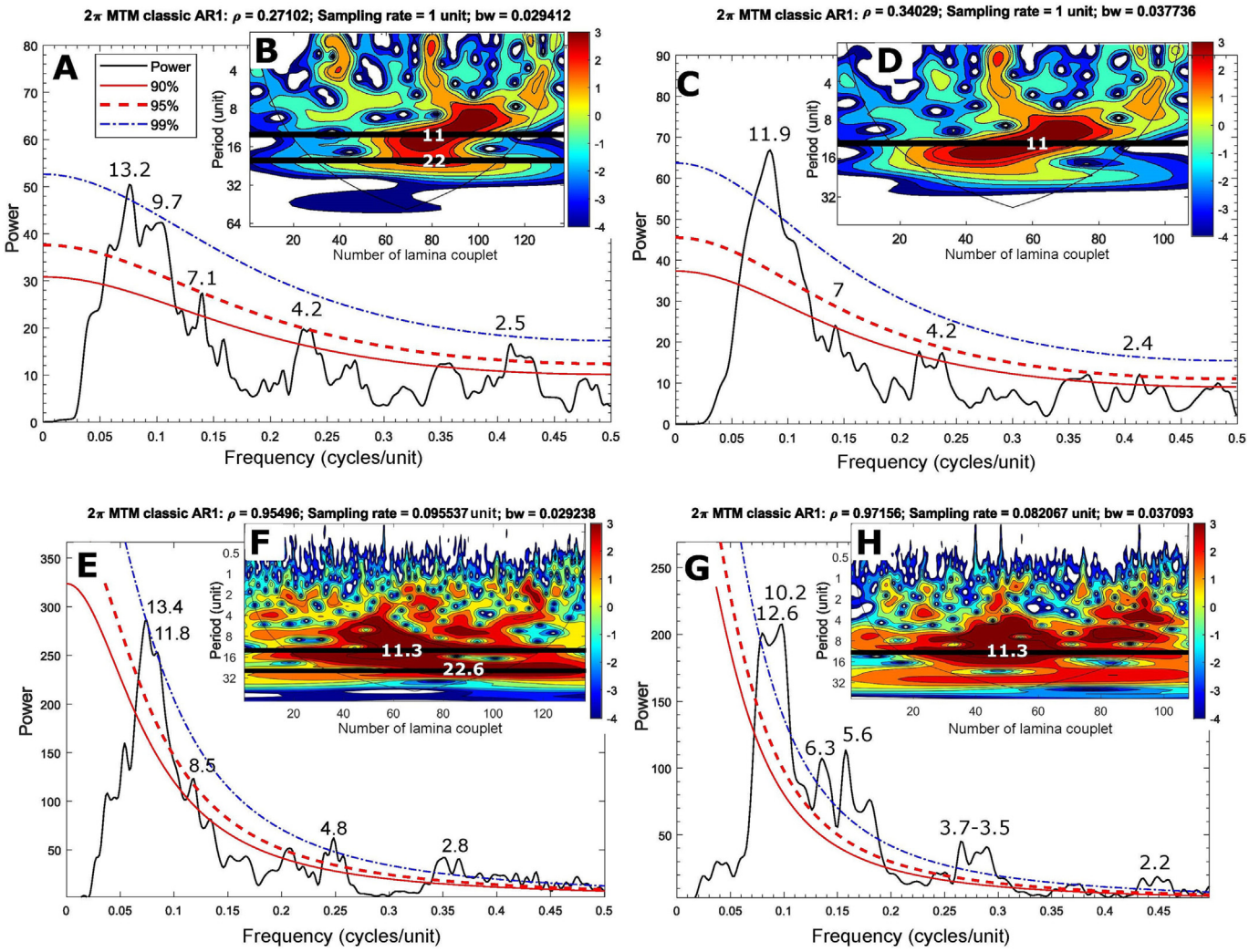

Fig. 13. Representative spectral and continuous wavelet analyses of specimen VD-13: A) 2π MTM power spectrum from the thickness of lamina couplets (all segments); B) wavelet spectrum from the thickness of lamina couplets (all segments); C) 2π MTM power spectrum from the thickness of lamina couplets (removed segment 2 values); D) wavelet spectrum from the thickness of lamina couplets (removed segment 2 values); E) 2π MTM power spectrum from raw luminance data from the same thickness measurement segments as in A; F) wavelet spectrum from raw luminance data obtained from the same thickness measurement segments as in C; G) wavelet spectrum from raw luminance data (removed segment 2 values); H) wavelet spectrum from raw luminance data (removed segment 2 values). The term "units" corresponds to the time interval represented by a couplet formed of a dark lamina plus a light lamina.

the noise in the periodicity of the lower frequencies, but at the same time makes it more difficult to recognise frequencies around 22.

Thus, the differences found between the results of the spectral analyses of VD-13A and VD-13B suggest that the deleted segment (i.e. segment 2) is not recording the simple lamination but a higher order one.

6. Discussion

6.1. Significance of structure and texture variations in the microbial lamination

The cyclic lamination pattern is typically interpreted in terms of climate and climate-dependent parameters, primarily temperature and precipitation and varying microbial activities (Golubic, 1991; Chafetz et al., 1991; Casanova, 1994; Adachi et al., 2017). Changes in depth and salinity, usually dependent on temperature and the precipitation/evaporation ratio, also explain some lacustrine microbial laminations (Lindqvist, 1994; Martin-Bello et al., 2019a). Variations in the water parameters such as temperature, and Ca^{2+} and HCO_3^- concentrations, as well as CO_2 content, which affect the SIc of water, are drivers of the textural variations between laminae (Martin-Bello et al., 2019b). Collectively, many studies on ancient and recent laminated microbialites support the notion that high SIc favours the formation of dense small-crystal textures, promoted during warm temperature conditions, in contrast to porous, large-crystal textures, which result from lower SIc values during cool temperature conditions (Arp et al., 2001; Gradziński, 2010; Arenas and Jones, 2017). Moreover, these textural changes can be produced within 1 year, as documented by studies of recent microbial sediments (Kano et al., 2007; Manzo et al., 2012; Arenas et al., 2014). Therefore, for micritic microbialites (*fine-grained stromatolites*, sensu Riding, 2000), as in the study example, the textural variations recorded by simple laminae were primarily linked to changes in the SIc and microbial mat development, primarily as a function of precipitation (or water inputs) and temperature variations through time.

In the studied oncolites, the dense dark micrite laminae, corresponding to light-coloured laminae in the polished sample (Fig. 6), formed under high calcite saturation levels during less rainy seasons and/or warm conditions. The microspar to spar laminae, corresponding to dark-coloured laminae in the polished sample, represent calcite precipitation under lower saturation levels than the dense dark micrite laminae during rainy seasons and/or cool conditions. The light porous micrite and/or microspar laminae, corresponding to light-coloured,

poorly laminated intervals in the polished sample, could have formed under conditions favouring animal bioturbation, affecting the microbial mat. Excluding the latter case, which was not considered for the diverse analyses, each light–dark couplet was interpreted to represent a 1-year deposit, with the constituent laminae attributed to seasonal temperature and/or precipitation changes. The composite laminae should then record variations in the same parameters over longer periods (e.g. multi-annual cycles). A similar interpretation of the Miocene lacustrine stromatolites in the Ebro Basin is found in Martin-Bello et al. (2019a, 2019b).

In mid-latitude regions, such as the Ebro Basin during the Miocene, seasonal changes in temperature and precipitation would be sufficiently contrasted to provoke a physiological response of the microbial mats, as proposed by Casanova (1994) with the concept of 'ecological cycles'. These changes could cause variations in the calcite saturation levels in the lake water, leading to varying textural features according to seasonal physicochemical and biological variations. These arguments support the formation of dense dark micrite laminae in warm and/or dry conditions and dense-to-porous light micrite and spar laminae in cool and/or wet conditions. Microbial bodies are present in both laminae, indicating that microbial growth was not interrupted during the time represented by the laminae. These interpretations also agree with the stable isotopic composition of the laminae in specimen C4-31. According to the temperature dependence of oxygen fractionation during calcite precipitation (Faure, 1998; Osácar et al., 2013), the mean isotopic values of C4-31 are consistent with the formation of dense dark micrite laminae during the warm seasons, and the microspar and spar laminae during the cool seasons. However, these interpretations must be taken cautiously because the mean isotopic difference between the textural types is small.

6.2. Discontinuities in the oncolite coatings

The large continuity and uniform thickness of the oncolite laminae are typical features close to the nuclei, corresponding to the youngest growing phases. These features are related to the continuous motion of grains in shallow lakes or gentle fluvial currents. The high porosity and low density of oncolites favour the movement of oncolites compared with limestone clasts of equivalent hydraulic diameter under similar water energy conditions (Verrecchia et al., 1997). This difference allows continuous growth of microbial mats around the entire nuclear particle. Once a given size is reached, the oncolites remain still for a long time, considering invariable hydraulic conditions, until strong water movement or flood events cause them to move again. During oncolite grounding (not moving), two scenarios may occur: 1) the younger laminae can be affected by erosion owing to other grains transported by the current affecting them, and 2) in the absence of other grains affecting them, the ongoing growth of microbial mats occurs on the exposed surface under still or slow-moving water. In both cases, the oncolites acquired irregular shapes, with some incomplete laminae. These laminae may be highly porous because of the diverse morphological types of individual and grouped cyanobacteria (framework porosity), and aquatic invertebrate animal colonisation (e.g. insect larvae and small crustaceans). Porosity due to invertebrate activities has been described in other fluvial oncolites (Zamarreño et al., 1997; Arenas et al., 2007). Fig. 14 shows a possible reconstruction story of the initial growth stages of an oncolite based on the discontinuities recognised through lamination in one of the study sections.

6.3. Climatic and hydrological significance of the $\delta^{13}C$ and $\delta^{18}O$ values

Vázquez-Urbez (2008) proposed that the deposition of Unit T7 in the Borja–Tarazona region, including the oncolite C4-31 bearing layer, occurred in a small marginal lake system that flowed either via surface or underground towards closed lacustrine areas in the centre of the Ebro Basin. The residence time of water in the marginal lake system would be sufficiently long to reach a significant correlation between $\delta^{13}C$ and $\delta^{18}O$, as inferred from the isotope values of all carbonate facies in Unit T7 of that region ($r = 0.41$, $N = 52$).

The $\delta^{13}C$ and $\delta^{18}O$ values of specimen C4-31 roughly represent the depositional and climatic conditions during light and dark lamina formation, corresponding to varied temporal spans. These $\delta^{13}C$ and $\delta^{18}O$ values (Table 1; Figs. 8, 9) are typical of meteoric water with little evaporative effects and with CO_2 derived from soils (cf. Andrews, 2006). Moreover, the slight variation in $\delta^{18}O$ values over time and the absence of correlation between $\delta^{13}C$ and $\delta^{18}O$ ($r = 0.08$, $N = 43$) indicate a hydrologically open sedimentary setting (cf., Leng and Marshall, 2004; Cyr et al., 2005) for depositing the oncolite-bearing layer. The absence of correlation between the $\delta^{13}C$ and $\delta^{18}O$ values in oncolite C4-31 could be related to an episode of water recharge, with the consequent expansion and overflow of the marginal lake during which the thick marl-matrix oncolite layer containing the studied oncolites would be deposited. This scenario did not favour the evaporative effects on the lake water, which would have had an isotopic composition closer to meteoric water than the rest of the time (i.e. during low lake levels). Thus, the C4-31 oncolite values would reflect a dilute lake-water situation by more negative values of $\delta^{13}C$ and $\delta^{18}O$ (the mean values are $\delta^{13}C = -7.49$ ‰ V-PDB and $\delta^{18}O = -8.93$ ‰ V-PDB) than the rest of Unit T7, to which Vázquez-Urbez (2008) calculated mean values of $\delta^{13}C = -7.10$ ‰ V-PDB and $\delta^{18}O = -7.83$ ‰ V-PDB.

In oncolite C4-31, spanning approximately 150 years based on counting couplets, each considered to represent 1 year, the isotopic values show minor variations over time, which could be interpreted in terms of temperature and precipitation/evaporation. Fig. 9 shows one interval with the most negative $\delta^{18}O$ values (samples 24–36), which might be attributed to periods of warm temperatures and/or a high precipitation/evaporation ratio (P/E) within an overall evolution towards warming and/or humid conditions over time. For $\delta^{13}C$, samples 33–38 form an interval with the most negative values related to increasing precipitation periods when organic-derived CO_2 input was higher. In the aforementioned intervals, $\delta^{13}C$ and $\delta^{18}O$ variations are not simultaneous; instead, the $\delta^{18}O$ decrease precedes the $\delta^{13}C$ decrease. In the interval comprising samples 13–19, $\delta^{13}C$ and $\delta^{18}O$ had the least negative values. This isotopically less negative interval is mostly formed of by dark micrite-dominated intervals, except for a light, poorly laminated group of laminae at the base that might have dominantly formed during high precipitation and/or cool temperature conditions (Figs. 6A, 9).

The oncolite-bearing beds of Unit T8 and beds containing other facies that compose this unit formed under humid conditions, as inferred by Vázquez-Urbez (2008) from the low $\delta^{13}C$ values ($\delta^{13}C = -7.93 \pm 0.45$; $N = 44$), compared to those of the underlying Unit T7 ($\delta^{13}C = -7.02 \pm 1.34$; $N = 52$), and the abundant *calcite-coated* plants, as debris and in situ, that would have formed in extensive palustrine areas within the fluvial–lacustrine system. Notably, growth rate estimates (considering one lamina couplet per year) show that specimen VD-13 grew faster (0.26 mm y^{-1}) than specimens C4-1 and C4-31 (0.20 mm y^{-1}), consistent with the high deposition rates typically occurring in fluvial carbonate environments. Likewise, specimen VD-13 contains evidence of intense bioturbation, indicating rich aquatic life during Unit T8 deposition. However, these interpretations should be treated cautiously, as the diagenesis reset of the isotope signature cannot be excluded despite the pristine sampling procedure.

6.4. Recognition of solar activity and atmospheric circulation cycles in the oncolite lamination

The spectral analysis results reveal the persistence of spectrum peaks (above the 99 % confidence level) at the same period bands: around periods 2.5, 3 and 10–12 in the three specimens, and 19–23 in oncolite C4-31. Other peaks appear occasionally in the band between periods 5 and 7, depending on the specimen and the type of time-

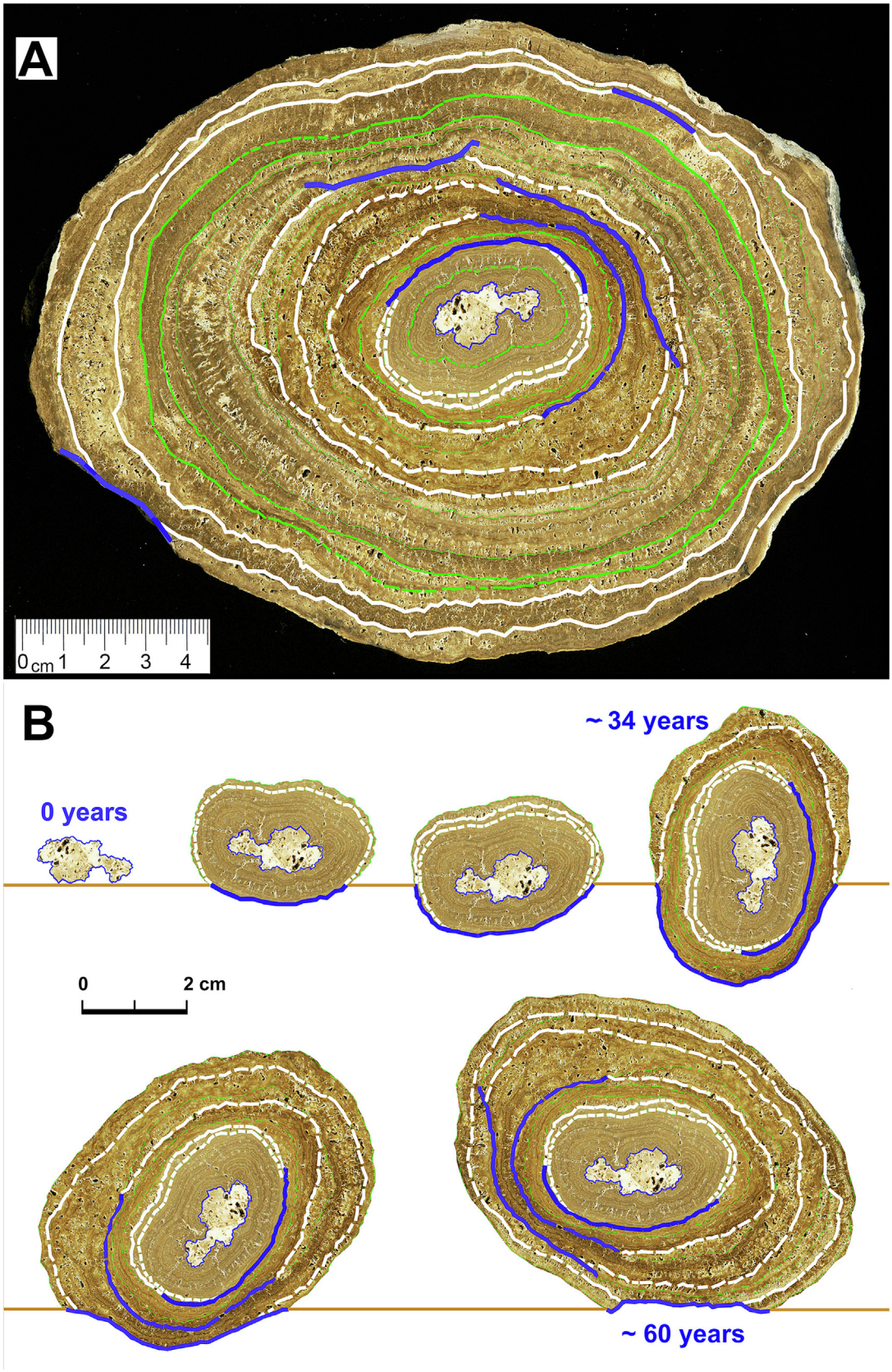

Fig. 14. Reconstruction of lamina development in oncolite VD-13. A) The white and green lines indicate several growing stages that separate time-equivalent intervals, and the blue lines correspond to areas where the oncolite growth was interrupted for several years, by grounding or erosion. B) Stages of lamina formation through approximately the first 60 years. A graphic representation has been performed considering that the oncolite remained stationary on the sedimentation surface for each vignette shown in the figure.

series. The analyses performed on raw luminance time-series, elaborated with 1000 and 2000 values, revealed significant peaks around periods 11 in C4-1 and VD-13, and 22 in C4-31.

On the hypothesis that each couplet formed of a simple light lamina plus a simple dark lamina represents 1 year, the obtained couplet periods equal years. The period around 2.5 years in the spectra might be related to the quasi-biennial oscillation (QBO, Baldwin et al., 2001). The period around 3 years is widely present and could be related to the typical frequencies of the ENSO phenomenon; however, other periods usually recognised as typical modes of ocean and/or atmospheric circulation phenomena as NAO and/or ENSO, around 5 and 7 years (Quinn and Neal, 1987; Philander, 1990; Hurrell and van Loon, 1997; Weedon, 2003), are only occasionally recognised in the spectra. The presence of peaks representing 9.7–12.6 and 18.7–22.6 years was outstanding. The former group (hereafter, 10–13) correlates with the 11-year Schwabe sunspot cycle. This solar cycle has a quasi-periodic recurrence with a mean of approximately 11 years, and its duration varies with a standard deviation of approximately 14 months (Hathaway, 2015). The group with 18.7–22.6-year variability (hereafter, 19–23), well represented in the C4-31 spectra, can be linked to the 22-year Hale sunspot cycle.

The cycles recognised at 10–13 and 19–23 years can also be attributed to the low-frequency modes of the atmospheric circulation patterns of the NAO (Rossi et al., 2011; Ólafsdóttir et al., 2013) and ENSO (Zhang et al., 1997; Cook, 2000). However, the rare occurrence in the spectral analysis of significant spectral peaks at typical frequency bands (between 5 and 7 years) of the aforementioned circulation phenomena (Quinn and Neal, 1987; Philander, 1990; Hurrell and van Loon, 1997; Weedon, 2003) indicates a direct influence of solar activity rather than a NAO or ENSO-like influence on the lamina development of the oncolites in this study.

Lamina counting revealed that some intervals possess 9–13 simple lamina couplets (the white segments shown in Fig. 15). Likewise, these intervals can be arranged into light–dark couplets (19–23 simple lamina couplets, the black lines shown in Fig. 15), fitting composite lamina couplets. These cycles can be recognised clearly in the middle portion of specimen C4-31. This visual pattern was consistent with the spectral analysis results (Fig. 10). The approximately 11 simple lamina couplets might correspond to the 11-year Schwabe solar cycles (the white segments shown in Fig. 15), whereas each light–dark composite lamina couplet (the black lines shown in Fig. 15) might be related to the 22-year Hale solar cycles. Together, these results are consistent with the hypothesis of a 1-year duration for each lamina couplet.

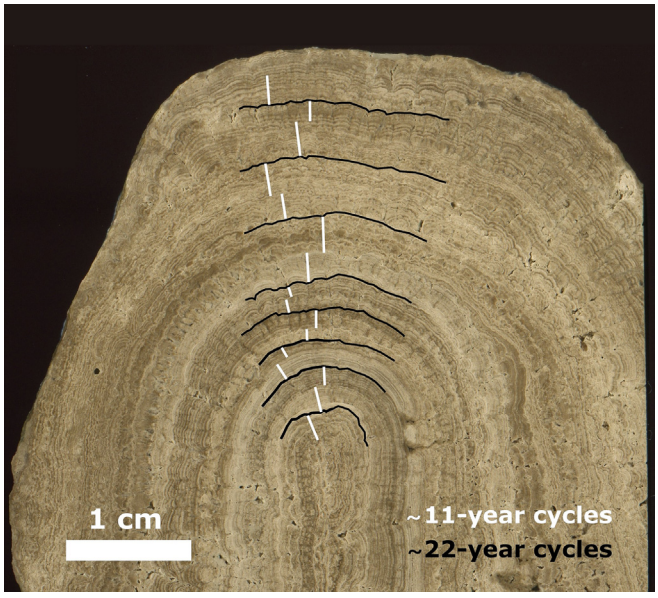

Fig. 15. Recognition of quasi-periodic sunspot cycles over the distribution of lamina couplet thickness of specimen C4-31: 11-year Schwabe sunspot cycles (white lines) and 22-year Hale sunspot cycles (black lines).

Regarding the results based on the C and O isotope values of the C4-31 specimen, the temporal series used in the spectral analysis was performed only with 43 data points. A small sample size causes high-frequency components corresponding to the lowest periods recorded by the thicknesses and luminance spectra not to be reflected in the isotope spectral analysis. Additionally, irregular sampling, that is, the sampled points include several simple laminae (3 to 13), could have caused the obtained isotopic values to represent a mixture of signatures of different durations. This circumstance implies the appearance of aliasing effects (Priestley, 1981; Weedon, 2003). This phenomenon means that the power spectrum of the primary peak leaks into the side frequencies, producing worse differentiation of the cycle frequencies than those of the spectra from longer and regularly sampled time-series. In brief, irregular and scarce sampling makes obtaining a precise spectral analysis challenging.

Despite this limitation, the clusters of significant periods around 10.8 (9.2–11.6-year; Fig. 11A) in the $\delta^{18}O$ spectrum and around 13.3 (12–14.7-year; Fig. 11B) in the $\delta^{13}C$ spectrum might reflect the 11-year Schwabe cycle. Likewise, the most significant peaks at the 20.9-year ($\delta^{18}O$; Fig. 11A) and 22.9-year ($\delta^{13}C$; Fig. 11B) periods match the 22-year Hale sunspot cycle. Although the precision of these peaks is not optimal, the occurrence of these particular frequencies in the spectra and not others in $\delta^{13}C$ and $\delta^{18}O$ indicates the credibility of the aforementioned relationship between the stable isotope values and the solar activity cyclicity. Moreover, the coincidence of these results with those obtained from the lamina thickness reinforces the correlation between the lamina thickness and solar activity, specifically the quasi-periodic periodicity of the sunspots.

The influence of periodic climatic variations on the development of laminae differs depending on their composition and/or depositional context. For the siliciclastic bio-laminites of the Wuqlangxi Formation (Li et al., 2018), the warm seasons (late spring to autumn) produce thin, organic-rich, argillaceous dark laminae. However, cool conditions (winter to early spring) contribute to the thick, organic-poor, silty–sandy light lamina deposition. Although microbial activities influenced by temperature and precipitation variations contributed to the lamina thickness of the organic-rich argillaceous dark laminae, the dominant factor in thickness variations in lamina couplets was the siliciclastic inputs in the silt–sand-rich light laminae due to continental weathering and surface runoff. For the Eocene lacustrine fine-grained rocks of the Bohai Bay Basin (Shi et al., 2021), warm conditions were suitable for carbonate precipitation, resulting in thick light laminae composed primarily of calcite, and humid and cold conditions favoured the development of thick dark laminae composed primarily of fine clay minerals, organic matter, and quartz debris. The relative variation in the thicknesses of the lamina couplet records the variability of the 11-year Schwabe sunspot cycle. In this Eocene and other aforementioned cases focusing on the fluvial and lacustrine microbial carbonate lamination (Casanova, 1986, 1994; Lindqvist, 1994; Arp et al., 2001; Arenas et al., 2015; Martin-Bello et al., 2019a, 2019b; Pérez-Rivarés et al., 2019), precipitation and temperature variations have been proposed to control the thickness variations in the light–dark couplets. However, the examples of fluvial and lacustrine microbial carbonate lamination indicate that the rhythmic pattern results from dense micrite laminae formed during dry seasons and/or warm conditions, and porous micrite and/or microspar laminae are formed during high precipitation and/or cool periods. Regardless of the lamina origin, in all cases that have performed periodic studies, the cyclical behaviour was consistent with the periodic or quasi-periodic variations in solar activity, as found in this case study.

A spectral analysis of the lamination periodicity similar to that in this study was implemented in lacustrine stromatolites formed in the Early–Middle Miocene in the same basin (Pérez-Rivarés et al., 2019). Thickness variations in the light–dark couplets in the stromatolites seemed to be controlled by the periodic changes in precipitation and

temperature influenced by NAO/ENSO-like variability, and could be related directly to 11-year solar cycles. However, in the oncolites considered herein, the influence of solar irradiation (11-year Schwabe solar cycles) is best represented in the spectral analysis, whereas the effect of NAO/ENSO-like cycles is the least evident.

The differences in the results obtained from the cyclicity analyses of both types of microbial deposits could be associated with the shape of laminae in oncolites and stromatolites, which may affect the thickness measurements. Oncolites show common lateral changes in lamina thickness and crenulated outlines, resulting in a lower regularity in continuity compared to the stromatolitic laminae. In addition, the boundaries between laminae are generally sharper in the stromatolites than in the oncolites. This aspect makes the lamina boundaries more precisely identifiable in the stromatolites. The distinct depositional and hydrological conditions in which these two groups of microbialites formed, primarily the water depth and flow conditions, and the open versus closed hydrology of the water bodies, could have influenced lamina thickness variations and hence the recording of cyclic changes. Notably, the microbial structures (i.e. microbial bodies) preserved in oncolites and stromatolites differ morphologically, responding to changes in water salinity and hydrodynamic conditions. These morphologically different microbial compositions can produce notable changes in the lamina shapes (Arenas-Abad, 2022). All these features can influence lamina thickness estimates.

Another differential factor affecting the dominant cyclicity reflected by oncolites and stromatolites might be related to the presence of hiatuses through the laminated record that are linked to the mobile versus steady development of the microbialites. It seems reasonable to think that the mobility of oncolites can cause a greater profusion of non-growth or erosion situations in the resulting lamination compared to the stromatolite lamination. Nevertheless, both types of microbial lamination show periodic growth patterns comparable to typical modes of the solar activity variability and maybe also to those of climate circulation phenomena such as NAO or ENSO.

7. Conclusions

Periodicity analysis performed on three Miocene lacustrine and fluvial oncolites in the Ebro Basin, Spain, allowed the detection of lamina cycles that could be related to solar activity. The analysis was performed using three spectral analysis methods (multi-taper, smoothed periodogram, and wavelet analysis) and two types of data (lamina thickness and luminance) on the three specimens. This redundant methodology proved that the persistent cyclicity encountered at several shared frequencies does not respond to a random factor in the data series. The results revealed periods with high confidence levels (>95 %). Each simple light–dark lamina couplet corresponding to textural variations linked to crystal size and porosity was hypothesised to represent 1 year. The following conclusions can be drawn:

- The premise of annual duration for each simple light–dark lamina couplet is consistent with the textural variation of the laminae and has allowed the calculation of oncolite growth rates, which vary between 0.20 and 0.26 mm y^{-1}. These values are within the range calculated for other Miocene microbialites in the Ebro Basin.
- Time-series analysis based on the thickness of simple lamina couplets showed persistent significant periods around 2.5, 3 and 10–13 in the three studied specimens. These periods can be associated with the typical oscillations of specific climatic signatures. The 2.5-year periods correspond to the QBO or the biennial component of ENSO or NAO variability. Periods 10–13 can be linked to the 11-year Schwabe sunspot cycles. Other periods around 5, 7 and 22 years are only present in some spectra. Although the 3-, 5- and 7-year periods are typical modes of ENSO or NAO variability, their credibility is doubtful because they are not present in all specimens. Periods 19–23, present in the C4-31 specimen, match the 22-year Hale solar cycle.
- The spectral analysis based on $\delta^{13}C$ and $\delta^{18}O$ values yielded periods of approximately 10–13 and 19–23 years, respectively, which correlate to the 11-year Schwabe and 22-year Hale solar cycles.
- The agreement of the periodicity results obtained from the three methods and the consistency of the calculated growth rates support the hypothesis that the lamina-couplet duration is 1 year.
- The diverse results indicate that solar irradiance variations influenced the characteristics of the oncolite laminae, particularly through temperature, precipitation and light availability fluctuations. Therefore, this study provides further evidence of the utility of high-resolution records from microbial laminations for understanding the influence of climate on short-time sedimentation cycles.

Supplementary data to this article can be found online at https://doi.org/10.1016/j.sedgeo.2023.106563.

CRediT authorship contribution statement

F.J. Pérez-Rivarés: Conceptualization, Data curation, Formal analysis, Investigation, Methodology, Writing – original draft, Writing – review & editing. **G. Pardo:** Conceptualization, Data curation, Formal analysis, Investigation, Writing – original draft, Writing – review & editing. **C. Arenas:** Conceptualization, Data curation, Formal analysis, Funding acquisition, Investigation, Project administration, Writing – original draft, Writing – review & editing.

Data availability statement

The data that support the findings of this study are available in the Supplementary material of this article. Additional data are available on request from the authors.

Declaration of competing interest

The authors declare that they have no known competing financial interests or personal relationships that could have appeared to influence the work reported in this paper.

Acknowledgements

Financial support for this work was provided by the Spanish Ministry through grants CGL2013-42867-P and PID2019-106440GB-C22 (MCIN/AEI 10.13039/501100011033). The authors would like to acknowledge the Servicio General de Apoyo a la Investigación-SAI, Universidad de Zaragoza, Spain, and the Servicios Científico-Técnicos (CCIT-UB Serveis), University of Barcelona. We are grateful to Marta Vázquez-Urbez for providing information regarding the study area. Paulina Leonowicz and an anonymous reviewer, as well as the Editor-in-Chief C. Chagué, helped improve the manuscript. This contribution is dedicated to the memory of our colleague and friend Arsenio Muñoz Jiménez, who passed away in September 2022. He was an enthusiastic pioneer of cyclostratigraphy in the lacustrine sequences of the northeast Iberian Peninsula.

References

Adachi, N., Asada, Y., Ezaky, Y., Liu, J., 2017. Stromatolites near the Permian–Triassic boundary in Chongyang, Hubei Province, South China: a geobiological window into palaeo-oceanic fluctuations following the end-Permian Extinction. Palaeogeography, Palaeoclimatology, Palaeoecology 475, 55–69.

Andrews, J.E., 2006. Palaeoclimatic records from stable isotopes in riverine tufas: synthesis and review. Earth-Science Reviews 75, 85–104.

Arenas, C., Jones, B., 2017. Temporal and environmental significance of microbial lamination: insights from recent fluvial stromatolites in the River Piedra, Spain. Sedimentology 64, 1597–1629.

Arenas, C., Cabrera, L., Ramos, E., 2007. Sedimentology of tufa facies and continental microbialites from the Palaeogene of Mallorca Island (Spain). Sedimentary Geology 197, 1–27.

Arenas, C., Vázquez-Urbez, M., Auqué, L., Sancho, C., Osácar, C., Pardo, G., 2014. Intrinsic and extrinsic controls of spatial and temporal variations in modern fluvial tufa sedimentation: a thirteen-year record from a semi-arid environment. Sedimentology 61, 90–132.

Arenas, C., Piñuela, L., García-Ramos, J.C., 2015. Climatic and tectonic controls on carbonate deposition in syn-rift siliciclastic fluvial systems: a case of microbialites and associated facies in the Late Jurassic. Sedimentology 62, 1149–1183.

Arenas-Abad, C., 2022. A multi-scale approach to laminated microbial deposits in non-marine carbonate environments through examples of the Cenozoic, north-east Iberian Peninsula, Spain. The Depositional Record 8, 67–101.

Arp, G., Wedemeyer, N., Reitner, J., 2001. Fluvial tufa formation in a hard-water creek (Deinschwanger Bach, Franconian Alb, Germany). Facies 44, 1–22.

Baldwin, M.P., Gray, L.J., Dunkerton, T.J., Hamilton, K., Haynes, P.H., Holton, J.R., Alexander, M.J., Hirota, I., Horinouchi, T., Jones, D.B.A., Marquardt, C., Sato, K., Takahashi, M., 2001. The Quasi-Biennial Oscillation. Reviews of Geophysics 39, 179–229.

Bradley, W.H., 1929. The varves and climate of the Green River epoch. U.S. Geological Survey Professional Paper 158, 87–110. https://doi.org/10.3133/pp158E.

Bradley, W.H., 1931. Origin and microfossils of the oil shale of the Green River Formation of Colorado and Utah. U.S. Geological Survey Professional Paper 168, 1–58. https://doi.org/10.3133/pp168.

Brasier, A.T., Andrews, J.E., Marca-Bell, A.D., Dennis, P.F., 2010. Depositional continuity of seasonally laminated tufas: implications for δ18O based palaeotemperatures. Global and Planetary Change 71, 160–167.

Casanova, J., 1986. East African Rift stromatolites. In: Frostick, L.E., Renaut, R.W., Reid, I., Tiercelin, J.J. (Eds.), Sedimentation in the African Rifts. Geological Society, London, Special Publications vol. 25, pp. 201–210.

Casanova, J., 1994. Stromatolites from the East African Rift: a synopsis. In: Bertrand-Sarfati, J., Monty, C. (Eds.), Phanerozoic Stromatolites II. Kluwer Academic Publishers, pp. 193–226.

Chafetz, H.S., Utech, N.M., Fitzmaurice, S.P., 1991. Differences in the δ 18O and δ 13C signatures of seasonal laminae comprising travertine stromatolites. Journal of Sedimentary Petrology 61, 1015–1028.

Cook, E.R., 2000. Niño 3 Index Reconstruction. International Tree-Ring Data Bank. IGBP PAGES/World Data Center-A for Paleoclimatology. Data Contribution Series #2000-052. NOAA/NGDC Paleoclimatology Program, Boulder, CO, USA.

Costa, E., Garces, M., López-Blanco, M., Beamud, E., Gómez-Paccard, M., Larrasoaña, J.C., 2010. Closing and continentalization of the South Pyrenean foreland basin (NE Spain): magnetochronological constraints. Basin Research 22 (6), 904–917.

Crowley, T.J., Short, D.A., Mengel, J.G., North, G.R., 1986. Role of seasonality in the evolution of climate during the last 100 million years. Science 231 (4738), 579–584. https://doi.org/10.1126/science.231.4738.579.

Cyr, A.J., Currie, B.S., Rowley, D.B., 2005. Geochemical evaluation of Fenghuoshan Group lacustrine carbonates, north-central Tibet: implications for the paleoaltimetry of the Eocene Tibetan Plateau. Journal of Geology 113, 517–533.

Faure, G., 1998. Principles and Applications of Geochemistry. Prentice Hall Inc., New Jersey, USA.

Golubic, S., 1991. Modern stromatolites: a review. In: Riding, R. (Ed.), Calcareous Algae and Stromatolites. Springer, Berlin, Heidelberg, pp. 541–561 https://doi.org/10.1007/978-3-642-52335-9_23.

Gradziński, M., 2010. Factors controlling growth of modern tufa: results of a field experiment. In: Pedley, P.M., Rogerson, M. (Eds.), Tufas and Speleothems: Unravelling the Microbial and Physical Controls. The Geological Society, London, Special Publication vol. 336, pp. 143–191.

Hathaway, D.H., 2015. The solar cycle. Living Reviews in Solar Physics 12, 4. https://doi.org/10.1007/lrsp-2015-4.

Hurrell, J.W., van Loon, H., 1997. Decadal variations in climate associated with the North Atlantic Oscillation. Climate Change 36, 301–326.

Husson, D., 2014. MathWorks File Exchange: RedNoise_ConfidenceLevels. https://www.mathworks.com/matlabcentral/fileexchange/45539-rednoise_confidencelevels (with corrections by L.A. Hinnov).

Kano, A., Hagiwara, R., Kawai, T., Hori, M., Matsuoka, J., 2007. Climatic conditions and hydrological change recorded in a high-resolution stable-isotope profile of a recent laminated tufa on a subtropical island, southern Japan. Journal of Sedimentary Research 77, 59–67.

Kodama, K.P., Hinnov, L., 2015. Rock Magnetic Cyclostratigraphy. Wiley-Blackwell, Hoboken, New Jersey.

Leng, M.J., Marshall, J.D., 2004. Palaeoclimate interpretation of stable isotope data from lake sediment archives. Quaternary Science Reviews 23, 811–831.

Lenz, O.K., Wilde, V., Riegel, W., Harms, F.J., 2010. A 600 k.y. record of El Niño-Southern Oscillation (ENSO): evidence for persisting teleconnections during the Middle Eocene greenhouse climate of Central Europe. Geology 38, 627–630.

Li, P.B., Tang, D.J., Shi, X.Y., Jiang, G.Q., Zhao, X.K., Zhou, X.Q., Wang, X.Q., Chen, X., 2018. Sunspot cycles recorded in siliciclastic biolaminites at the dawn of the Neoproterozoic Sturtian glaciation in South China. Precambrian Research 315, 75–91. https://doi.org/10.1016/j.precamres.2018.07.018.

Li, M., Hinnov, L., Kump, L., 2019. Acycle: time-series analysis software for paleocli-mate research and education. Computers and Geosciences 127, 12–22.

Lindqvist, J.K., 1994. Lacustrine stromatolites and oncoids. Manuherikia Group (Miocene), New Zealand. In: Bertrand-Sarfati, J., Monty, C. (Eds.), Phanerozoic Stromatolites II. Kluwer Academic Publishers, Dordrecht, The Netherlands, pp. 227–254.

Manzo, E., Perri, E., Tucker, M.E., 2012. Carbonate deposition in a fluvial tufa system: processes and products (Corvino Valley — southern Italy). Sedimentology 59, 553–577.

Martin-Bello, L., Arenas, C., Andrews, J., Alonso-Zarza, A.M., Marca, A., 2019a. Multi-scale records of climate change in lacustrine stromatolites: insights from the Miocene Ebro Basin. Palaeogeography, Palaeoclimatology, Palaeoecology 530, 312–329.

Martin-Bello, L., Arenas, C., Jones, B., 2019b. Lacustrine stromatolites: useful structures for environmental interpretation — an example from the Miocene Ebro Basin. Sedimentology 66, 2098–2133. https://doi.org/10.1111/sed.12577.

McCrea, J.M., 1950. On the isotopic chemistry of carbonates and a paleotemperature scale. The Journal of Chemical Physics 18 (6), 849–857.

Merz-Preiß, M., Riding, R., 1999. Cyanobacterial tufa calcification in two freshwater streams: ambient environment, chemical thresholds and biological processes. Sedimentary Geology 126, 103–124.

Monty, C.L.V., 1976. The origin and development of cryptalgal fabrics. In: Walter, M.R. (Ed.), Stromatolites. Elsevier, Amsterdam, pp. 193–249.

Muñoz, A., Arenas, C., González, A., Luzón, A., Pardo, G., Pérez, A., Villena, J., 2002a. Ebro basin (northeastern Spain). In: Gibbons, W., Moreno, T. (Eds.), The Geology of Spain. The Geological Society, London, pp. 301–309.

Muñoz, A., Ojeda, J., Sánchez-Valverde, B., 2002b. Sunspot-like and ENSO/NAO-like periodicities in lacustrine laminated sediments of the Pliocene Villarroya Basin (La Rioja, Spain). Journal of Paleolimnology 27, 453–463.

Murelaga, X., Pérez-Rivarés, F.J., Vázquez-Urbez, M., Zuluaga, M., 2008. New biostratigraphic and paleoecologic data from the middle Miocene (Aragonian) from the Tarazona de Aragón area (Ebro Basin) Zaragoza province, Spain. Ameghiniana 45 (2), 393–406.

Ndiaye, M., Davaud, E., Ariztegui, D., Fall, M., 2012. A semi-automated method for laminated sediments analysis. Journal of Geosciences 3, 206–210.

Noffke, N., Awramik, S.M., 2013. Stromatolites and MISS—differences between relatives. GSA Today 23 (9), 4–9. https://doi.org/10.1130/GSATG187A.1.

Ólafsdóttir, K.B., Geirsdóttir, Á., Miller, G.H., Larsen, D.J., 2013. Evolution of NAO and AMO strength and cyclicity derived from a 3-ka varve-thickness record from Iceland. Quaternary Science Reviews 69, 142–154.

Osácar, C., Arenas, C., Vázquez-Urbez, M., Sancho, C., Auqué, L.F., Pardo, G., 2013. Environmental factors controlling the $\delta^{13}C$ and $\delta^{18}O$ variations of recent fluvial tufas: a 12-year record from the Monasterio de Piedra Natural Park (NE Iberian Peninsula). Journal of Sedimentary Research 83, 309–322. https://doi.org/10.2110/jsr.2013.27.

Pérez Rivarés, F.J., 2016. Estudio magnetoestratigráfico del Mioceno del sector central de la Cuenca del Ebro: Cronología, correlación y análisis de la ciclicidad sedimentaria. University of Zaragoza, pp. 1–281. https://zaguan.unizar.es/record/79504 (Ph.D. Thesis, in Spanish).

Pérez-Rivarés, F.J., Arenas, C., Pardo, G., Garcés, M., 2018. Temporal aspects of genetic stratigraphic units in continental sedimentary basins: examples from the Ebro basin, Spain. Earth-Science Reviews 178, 136–153.

Pérez-Rivarés, F.J., Martin-Bello, L., Arenas-Abad, C., 2019. Periodicity in stromatolitic lamination: a potential record of ENSO, NAO, and SUNSPOT in the Miocene lacustrine record of the Ebro Basin, Spain. Sedimentary Geology 390, 83–99.

El Niño, La Niña, and the Southern Oscillation. In: Philander, S.G.H. (Ed.), International Geophysics Series 46. Academic Press, London (293 pp.).

Priestley, M.B., 1981. Spectral Analysis and Time Series. Academic Press, London (890 pp.).

Quinn, W.H., Neal, V.T., 1987. El Niño occurrences over the past four and a half centuries. Journal de Geophysical Research 92, 14449–14461.

Riding, R., 2000. Microbial carbonates: the geological record of calcified bacterial–algal mats and biofilms. Sedimentology 47, 179–214.

Ripepe, M., Roberts, L.T., Fischer, A.G., 1991. ENSO and sunspot cycles in varved Eocene oil shales from image analysis. Journal of Sedimentary Petrology 61, 1153–1163. https://doi.org/10.1306/D4267857-2B26-11D7-8648000102C1865D.

Rossi, A., Massei, N., Laignel, B., 2011. A synthesis of the time-scale variability of commonly used climate indices using continuous wavelet transform. Global and Planetary Change 78, 1–13.

Shi, J.Y., Jin, Z.J., Liu, Q.Y., Fan, T.L., Gao, Z.Q., 2021. Sunspot cycles recorded in Eocene lacustrine fine-grained sedimentary rocks in the Bohai Bay Basin, eastern China. Global and Planetary Change 205, 103614. https://doi.org/10.1016/j.gloplacha.2021.103614.

Shunk, A.J., Driese, S.G., Dunbar, J.A., 2009. Late Tertiary paleoclimatic interpretation from lacustrine rhythmites in the Gray Fossil Site, northeastern Tennessee, USA. Journal of Paleolimnology 42, 11–24.

Suarez-Gonzalez, P., Quijada, I.E., Benito, M.I, Mas, R., Merinero, R., Riding, R., 2014. Origin and significance of lamination in Lower Cretaceous stromatolites and proposal for a quantitative approach. Sedimentary Geology 300, 11–27.

Tang, D., Shi, X., Jiang, G., 2014. Sunspot cycles recorded in Mesoproterozoic carbonate biolaminites. Precambrian Research 248, 1–16. https://doi.org/10.1016/j.precamres.2014.04.009.

Thomson, D.J., 1982. Spectrum estimation and harmonic analysis. Proceedings of the Institute of Electrical and Electronics Engineers 70, 1055–1096.

Thomson, D.J., 1990. Time series analysis of Holocene climate data. Philosophical Transactions of the Royal Society 330, 601–660.

Torrence, C., Compo, G.P., 1998. A practical guide to wavelet analysis. Bulletin of the American Meteorological Society 79, 61–78.

Vázquez-Urbez, M., 2008. Caracterización y significado ambiental de depósitos tobáceos neógenos de la Cuenca del Ebro. Comparación con ambientes Cuaternarios. Universidad de Zaragoza, pp. 1–476.. http://zaguan.unizar.es/record/2057/files/TESIS-2009-038.pdf (Ph.D. thesis, in Spanish).

Vázquez-Urbez, M., Arenas, C., Pardo, G., Pérez-Rivarés, J., 2013. The effect of drainage reorganization and climate on the sedimentologic evolution of intermontane lake systems: the final fill stage of the Tertiary Ebro Basin (Spain). Journal of Sedimentary Research 83, 562–590.

Verrecchia, E.P., Freytet, P., Julien, J., Baltzer, F., 1997. The unusual hydrodynamical behaviour of freshwater oncolites. Sedimentary Geology 113 (3–4), 225–243.

Walter, M.A., 1972. Stromatolites and the biostratigraphy of the Australian Precambrian and Cambrian. Special Papers in Palaeontology vol. 11. Palaeontological Association, London, p. 190.

Weedon, G.P., 2003. Time-series Analysis and Cyclostratigraphy. Cambridge University Press, Cambridge https://doi.org/10.1017/CBO9780511535482.

Zamarreño, I., Anadón, P., Utrilla, R., 1997. Sedimentology and isotopic composition of Upper Palaeocene to Eocene non-marine stromatolites, eastern Ebro Basin, NE Spain. Sedimentology 44, 159–176.

Zhang, Y., Wallace, J.M., Battisti, D.S., 1997. ENSO-like interdecadal variability: 1900–93. Journal of Climate 10 (5), 1004–1020.